ACS Catalysis

Research Article

Cite This: ACS Catal. 2018, 8, 7842−7860

pubs.acs.org/acscatalysis

Tuning Brønsted Acid Strength by Altering Site Proximity in CHA Framework Zeolites

Steven Nystrom,[†] Alexander Hoffman,[†] and David Hibbitts*

Department of Chemical Engineering, University of Florida, 1030 Center Drive, Gainesville, Florida 32611, United States

Supporting Information

ABSTRACT: This study examines how Brønsted acid strengths—as predicted by dispersion-corrected periodic DFT calculations of deprotonation energy (DPE), dehydrogenation energy (DHE), and NH_3 binding energy (NH_3 BE)—are affected by site proximity in proton-form zeolites and how adsorbates on one acid site alter the strength of nearby acids. Protons can bind to four distinct O atoms around the single crystallographically unique T-site of CHA, and all such locations were examined as bare and NH_3-occupied sites. Protons prefer to bind to O1 atoms and orient within the plane of six-membered-ring (6MR) structures of CHA. NH_4^+ cations show a strong preference for binding in 8MR windows; 6MR structures are too small to solvate them. These preferences govern proximity effects on acid strength, studied here by probing the strength of a Brønsted acid site while a second site is placed in 23 locations separated by 1−3 T-sites. Placing a second acid in the 6MR of CHA decreased DPE and NH_3 BE values for the first site by >10 kJ mol^{-1} because the proton of the second site stabilized the deprotonated site across the 6MR. Acid site-pairs across 8MR structures interact very little when the second acid is bare, as residual protons do not prefer to orient within 8MR. One location of the second acid stabilized the adsorbed proton without stabilizing the deprotonated state, resulting in a significantly weaker acid. All of these effects are altered when the second site is instead occupied by an adsorbed NH_3, which acts as a proxy for strongly bound reactive intermediates and cationic transition states. The strength of the first site is significantly weakened (DPE and NH_3 BE increases of >20 kJ mol^{-1}) when a second site is NH_3-occupied and placed in the 6MR because such structures are too small to effectively solvate NH_4^+ cations. Acid sites are strengthened, however, when second sites are NH_3-occupied and placed across 8MR windows, because they are appropriately sized to solvate the NH_4^+ cations that simultaneously interact with both deprotonated sites. The alteration of acid strength by acid site proximity therefore depends on the specific arrangement (not merely Al−Al distances), the structural motifs present (such as 6MR structures which allow protons, but not NH_4^+, to stabilize proximal conjugate base anions), and the status of proximal sites as vacant or occupied, which determines the distances over which cationic−anionic stabilizations of deprotonated sites can take place.

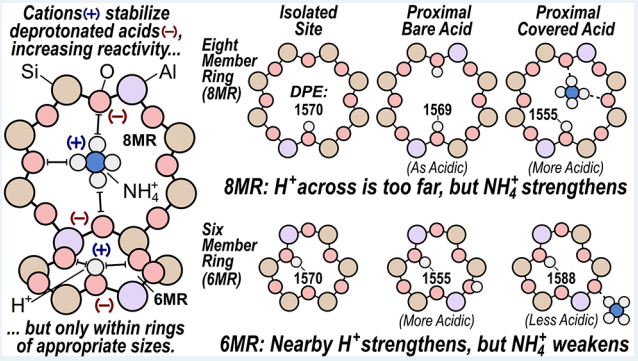

KEYWORDS: *zeolites, acid strength, Al distribution, density functional theory, Brønsted acid catalysis*

1. INTRODUCTION

Zeolites play a pivotal role in many industrially and academically relevant chemical processes,[1] such as catalytic cracking in the petrochemical industry,[2] methanol-to-hydrocarbons (MTH),[3−5] and separation processes.[6−8] Zeolites are microporous, crystalline aluminosilicates; over 200 frameworks have been synthesized[9−11] and another 350,000 frameworks have been theorized with formation energies within 30 kJ mol^{-1} of α-quartz, indicating stabilities within the range of synthesized materials.[12,13] The micropores which traverse zeolite crystals create diverse environments of varying void dimensions that affect reactivity and selectivity through size exclusion of reagents and transition states and differently confine and solvate reagents and transition states within the voids through noncovalent interactions.[14−18] Trivalent heteroatoms (Al^{3+}, Ga^{3+}, Fe^{3+}, B^{3+}) may substitute Si^{4+} at tetrahedral sites (T-sites) within the framework and create a net anionic charge that can be balanced by protons (H^+) located on adjacent O atoms, forming Brønsted acid sites. The energy required to fully separate the proton and form an anionic conjugate base is the deprotonation energy (DPE), a theoretical metric of the strength of an acid. Acid-catalyzed reactions typically resulting in charge separation of the acid site are therefore dependent on the DPE (acid strength) for reactions catalyzed by proton-form zeolites[15,19,20] and other well-defined solid-acid catalysts such as polyoxometalates (POM)[21−24] or even acid-promoted metal catalysts.[25−30] DPE is strongly influenced by the identity of the heteroatom in zeolite materials,[15,31] while the topology of the surrounding framework is believed to weakly affect DPE,[19] indicating that

Received: May 27, 2018
Revised: July 6, 2018
Published: July 12, 2018

DOI: 10.1021/acscatal.8b02049
ACS Catal. 2018, 8, 7842−7860

the observed effects of zeolite frameworks on reaction rates and selectivities are a consequence of their distinct local topographical environments rather than their acid strength—a subject of continued debate.[14,16−18,32−38]

The spatial density of Brønsted acid sites within aluminosilicate zeolites depends on the Si:Al ratio and the density of tetrahedral sites (framework density), and as the Brønsted acid site density increases, sites may be formed within close proximity to one another. New synthesis techniques are aimed at controlling the relative location and proximity of Brønsted acid sites within the zeolite framework.[39−45] The difference in acid strength and catalytic behavior between isolated acid sites and proximal sites is controversial, and these distinctions have been hampered by the inability to separate effects of bulk composition (Si:Al ratios) from the arrangement of Al sites in isolated or proximal configurations. Recently, synthesis and characterization techniques have been developed for many zeolites, including H-SSZ-13 (CHA framework), that control the fraction of Al sites within close proximity to one another by varying the ratio of two structure-directing agents (*N*,*N*,*N*-trimethyl-1-adamantylammonium and Na^+) without changing the Si:Al ratio.[39,40,46,47] These "paired" sites can then be counted using Co^{2+} titration methods that detect pairs of Al atoms within the same six-membered ring (6MR) of the CHA framework arranged in Al−O−(Si−O)$_x$−Al configurations with one to two linking Si atoms (x = 1, 2).[40] The arrangement of paired Al within 6MR structures of H-SSZ-13 is critical in the NO_x reduction on Cu-exchanged materials.[48−51] Synthesis techniques which vary Al distribution at constant Si:Al ratios and titrations which can count the number of paired sites enable kinetic measurements to determine the effects of Al site-pairing on chemical reactions. A probe reaction, methanol dehydration to dimethyl ether (DME), has been examined on these materials, and the results demonstrate that paired sites in CHA have proton-normalized rate constants (first and zero order) that are approximately 1 order of magnitude larger than isolated sites.[39] The exact cause of this enhancement is unknown; the second acid site in the paired configuration could (i) alter the local confinement effects by effectively reducing the local cage diameter (particularly if that second site has an adsorbate), (ii) stabilize cationic transition states formed at the first acid site via H-bonding or electrostatic interactions, or (iii) alter the acid strength of the first acid site through electronic effects (electron affinity of the conjugate base) or by H-bonding with the conjugate base. Here, we will examine the influence of acid site proximity on acid strength.

Rates of reactions often correlate strongly with DPE,[15,16,19,20,27] which is a purely theoretical assessment of acid strength given by calculating the reaction energy of heterolytically cleaving the O−H bond of the Brønsted acid:

$$\mathrm{H{-}Z} \rightarrow \mathrm{H^+} + \mathrm{Z^-} \tag{1}$$

where Z is the zeolite framework providing an O atom as the point of attachment for the proton. The energy of the anionic conjugate base (Z^-) is therefore required; periodic boundary conditions in density functional theory (DFT) result in dipole−dipole interactions between neighboring unit cells, which are exacerbated in charged calculations, as these have large dipole moments between the location of the anion and the uniform compensating background charge.[52] To overcome these issues, prior work has examined nonperiodic cluster models of zeolites,[31,53−55] which do not suffer from dipole−dipole interactions between neighboring unit cells but may not capture the effects of the framework. Similarly, hybrid methods coupling quantum and molecular mechanics (QM-MM) models use QM methods on a small active site regime and MM methods on the surrounding framework.[56−60] Recent work has calculated DPE for isolated acid sites in six zeolite frameworks using fully periodic DFT methods, and that work attempts to correct for periodic charge artifacts by recognizing a near-linear dependence between the DFT-calculated DPE values and the framework density of the framework, indicating that the charge artifacts may involve the framework density or perhaps—more simply—the size of the unit cell.[19] Previous work has noted that protons on proximal acid sites in an Al-rich framework can form intraframework H-bonds, which stabilize the Brønsted sites, or protons can destabilize one another via unfavorable electronic interactions, decreasing DPE.[61] Here, we will examine the effects of unit cell size and anion position on artifacts created by charged calculations in periodic DFT and demonstrate that the spatial density of the anion must be kept constant when DPE values are compared. In cases where it cannot be kept constant (comparing DPE across multiple frameworks), the anion density can be used as a more accurate correction factor than the framework density previously applied.[19]

To mitigate flaws inherent in charged periodic calculations, dehydrogenation energy (DHE) can be calculated in conjunction with DPE, which is the energy to homolytically cleave the O−H bond:

$$\mathrm{H{-}Z} \rightarrow \mathrm{H^\bullet} + \mathrm{Z^\bullet} \tag{2}$$

The difference in energy between the DPE and DHE is the sum of the ionization energy of a H atom ($H^\bullet \rightarrow H^+ + e^-$) and the electron affinity (EA) of the zeolite framework ($Z^\bullet + e^- \rightarrow Z^-$), which may depend on the local framework topology and composition (i.e., presence of another nearby Brønsted acid site).

Finally, acid strength can also be probed by the adsorption of a base, such as ammonia (NH_3), both experimentally and theoretically.[51,57,62−65] Theoretical base adsorption analysis is beneficial because charged calculations are avoided (like DHE and unlike DPE) while the O−H bond is heterolytically cleaved (like DPE and unlike DHE). However, the binding energy resulting from NH_3 adsorption and subsequent formation of NH_4^+ (NH_3 BE) will also be influenced by the surrounding cage topology through dispersive and H-bonding interactions;[62,64,66−68] therefore, NH_3 BE is not a "pure" metric of acid strength but measures a mixture of acid strength and confinement effects. For this reason, NH_3 TPD studies which aim to discriminate shifts in acid strength by shifts in desorption temperatures will give convoluted results.[1,19,66] Because NH_3 BE is influenced by the surrounding framework, however, it more accurately reflects the chemical behavior of reacting species, as shown in previous work for Brønsted acid catalyzed reactions.[27] Concurrent analysis of DPE, DHE, and NH_3 BE on H-form zeolites allows for a thorough description of the strength of Brønsted acids in these frameworks.

Here, we investigate acid strength in H-form CHA (H-SSZ-13) using DPE, DHE, and NH_3 BE with fully periodic DFT models for isolated Brønsted sites—with one acid site per unit cell—and for unit cells with multiple acid sites in 23 arrangements covering a wide range of Al−Al distances. For these configurations with multiple acid sites, we calculate the DPE, DHE, and NH_3 BE of an acid site while varying the

DOI: 10.1021/acscatal.8b02049
ACS Catal. 2018, 8, 7842−7860

location of a "second" site in the multisite configuration. We also examine the effects of coverage by recalculating DPE, DHE, and NH_3 BE for all Al-site arrangements while the second acid site is occupied by NH_3. Our results indicate that acid sites noticeably interact with one another at distances <9 Å (up to approximately three linking Si T-sites away) and that, within these distances, proximal acid sites may be stronger or weaker acids in comparison to isolated sites (evidenced by DPE, DHE, and NH_3 BE), depending on the exact arrangement of atoms. Critically, the "paired" sites within the 6MRs are stronger acids in comparison to isolated sites because the proton on the second acid site H-bonds with the conjugate base formed upon deprotonation of the first site and these are the same "paired" sites that dehydrate methanol at faster rates in CHA;[39] their enhanced acid strength provides a possible explanation for the observed rate enhancement. Acids are weakened by a second site when together they occupy nearby positions in the framework, but the proton on a second site cannot stabilize the conjugate base of a deprotonated site. The coverage of these sites also affects their acid strength, as enhancement in acid strength is greatest when the second acid site is a bare proton (and thus capable of H-bonding with the conjugate base of the first acid site), while the acid strength changes if the second acid site is occupied by an adsorbate, as they often are during catalytic reactions. This study therefore establishes the guiding principles necessary to tune acid strength through the formation of Al arrangements within interacting distances and can be used to guide the synthesis of such materials in CHA and other zeolite frameworks.

2. COMPUTATIONAL METHODS AND THE ARTIFACTS OF PERIODIC CHARGED CALCULATIONS

Fully periodic density functional theory (DFT) implemented in the Vienna ab initio simulation package (VASP)[69−72] determined the structures and energies for all states. Calculations were electronically converged to an energy difference between iterations of $<1.0 \times 10^{-6}$ eV and structurally converged such that the maximum force on any atom was <0.01 eV $Å^{-1}$, unless otherwise noted. Calculations were carried out with a plane wave energy cutoff of 400 eV, to form a basis set of projector augmented waves (PAW);[73,74] the revised Perdew−Burke−Ernzerhof (RPBE) exchange-correlation functional[75] was used along with the DFT-D3 with Becke−Johnson dampening to calculate dispersive forces and energies.[76] The BEEF functional[77,78] and PBE functional[79] with and without D3BJ were used to verify that trends in acid strength did not vary with choice of GGA by calculating DPE values with each functional; trends were in good agreement across all functionals (see Figure S7 in the Supporting Information). The Brillouin zone was sampled at the Γ point. Calculations for radical species were performed with spin polarization to account for unpaired electrons.

The CHA structure was acquired from the International Zeolite Association (IZA) database[80] (cell parameters $a = b = 1.3675$ nm, $c = 1.6675$ nm, $\alpha = \beta = 90°$, and $\gamma = 120°$); CHA contains one crystallographically unique T-site (36 total in the unit cell) and is shown in Figure 1 with a naming scheme for sites in the unit cell and identification of the four crystallographically unique O atoms attached to all T-sites. The framework has six distinct rings adjacent to each site: a 6MR, two 8MRs (one containing O2 and O3 atoms (8MR(2,3)) and one containing O2 and O4 atoms (8MR(2,4))), and three

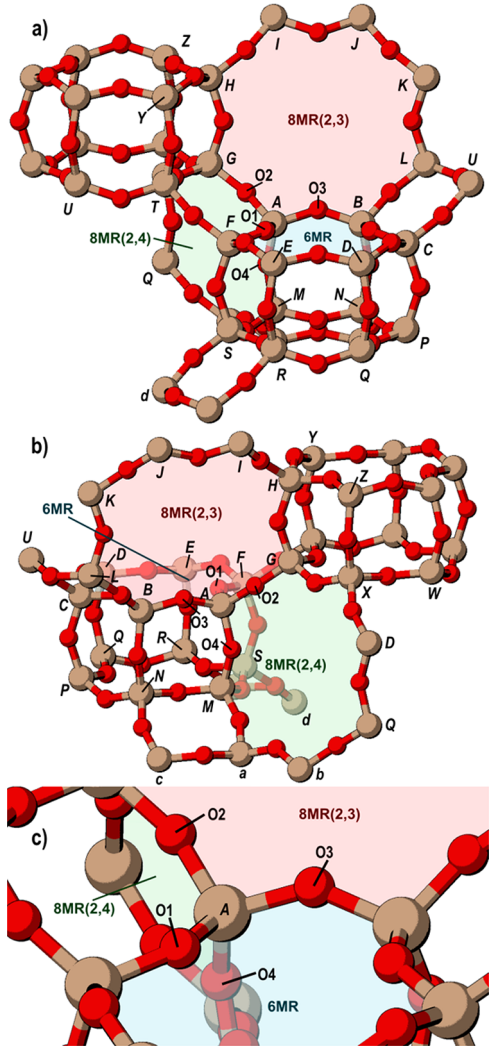

Figure 1. CHA framework. (a, b) Two views in which all T-site designations used in this study are labeled. Also shown and labeled are the 6MR and both 8MRs. (c) The four crystallographically unique O atoms and their location around the "first" T-site (designated here as site *A*). The rings labeled are according to the O atoms attached to the *A* site in each ring.

4MRs. The CHA structure was optimized, and no significant structural deviations were observed in comparison to the IZA structure.

DPE values were calculated as the difference in energy between the isolated charged species and the Brønsted acid site

$$\mathrm{DPE} = E_{Z^-} + E_{H^+} - E_{HZ} \quad (3)$$

and DHE values were calculated using neutral separated species

$$\mathrm{DHE} = E_{Z^\bullet} + E_{H^\bullet} - E_{HZ} \quad (4)$$

NH_3 BE calculations were obtained by calculating the energy difference of the NH_3-bound state (which always formed a cationic NH_4^+ species) and the proton-form zeolite:

$$E_{NH_3(ads)} = E_{Z-NH_4} - E_{HZ} - E_{NH_3} \quad (5)$$

The most stable structures and energies for each protonated state (HZ) were found by systematically placing the hydrogen on each of the four O atoms attached to an Al T-site. Optimization calculations were performed in which the H was

DOI: 10.1021/acscatal.8b02049
ACS Catal. 2018, 8, 7842−7860

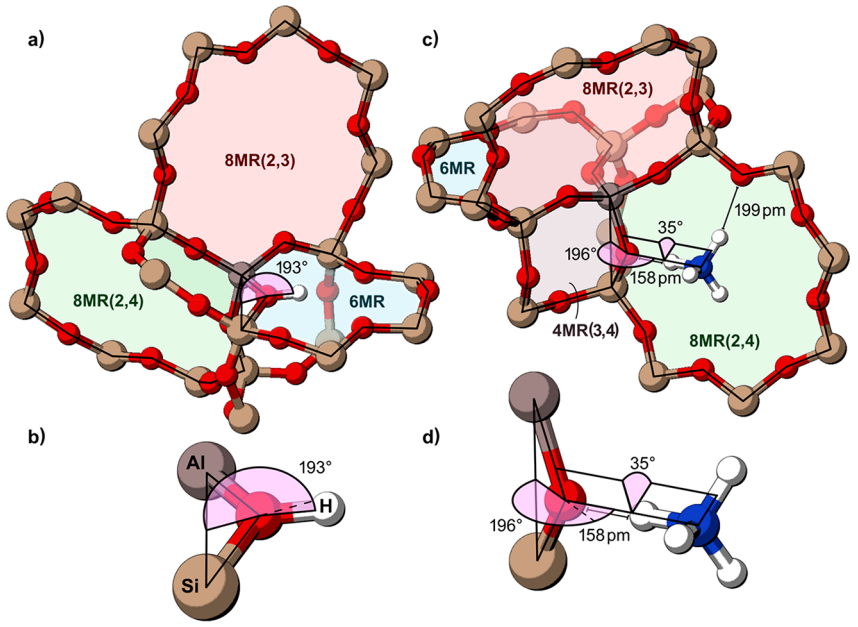

Figure 2. (a, b) Out-of-plane angle of a proton bound to the O1 atom of the T-site *A*. The most stable proton-form structure is depicted in which the proton rests in the 6MR of CHA. (c, d) Out-of-plane angle of NH_4^+ interacting with the O4 atom of T-site *A* and the Al−O−N−H torsional angle. The most stable NH_4^+-form structure is depicted in which the NH_4^+ rests in the 8MR comprised of O2 and O4 atoms (8MR(2,4)).

positioned 0.104 nm from each O and the out of plane angle of the H atom (Figure 2a,b) was varied from 0 to 330° in 30° intervals. This orientation sampling ensures that the most stable position of the H is obtained for each O atom location. Adsorbed proton species can rapidly move from one O atom to another via proton shuttling oxygenate species (e.g., NH_3, H_2O, CH_3OH, CH_3OCH_3);[16,81] therefore, a Boltzmann weighting at 415 K is used to produce an ensemble average energy for the protonated zeolite, $\langle E_{HZ} \rangle$, which accounts for this equilibration:

$$\langle E_{HZ} \rangle = \frac{\sum_{i=1}^{4} E_{HZ,i} \exp(-E_{HZ,i}/k_b T)}{\sum_{i=1}^{4} \exp(-E_{HZ,i}/k_b T)} \quad (6)$$

The arithmetic average of these states ($\overline{E_{HZ}}$) is also used in this work to describe the preferential siting of H on various O atoms and to describe averages across T-site locations, whose framework locations are not equilibrated. An ammonium ion (NH_4^+) was placed near each O atom of the negatively charged framework, and its orientation was systematically altered in search of the lowest energy configuration of the adsorbate. The out-of-plane angle of NH_4^+ was varied using methods similar to those used to rotate a proton around the O to which it was bound, and NH_4^+ was also rotated in 30° increments around the N−H bond oriented at the deprotonated O atom (Figure 2c,d).

Vibrational frequencies were determined by a fixed displacement method (two displacements) and used to calculate zero-point vibration energies (ZPVE) and temperature-corrected enthalpies (H) and free energies (G) at 415 K to determine if deprotonation potential energies (E) yielded trends significantly different from deprotonation enthalpies (H) or free energies (G). Frequency calculations froze all framework Si and O atoms that were not bound to the Al atom.

Proximity effects on acid strength were probed by replacing Si atoms 1−3 linking T-sites away from one another to generate Al−O−(Si−O)$_x$−Al sites (x = 1−3). Concurrent variations of the out-of-plane angles of both Brønsted sites would require 144 optimization calculations for the 12 angles probed on each site; these 144 configurational calculations were performed on the *AD* site-pair to test their necessity. The preferred out-of-plane H angles for all O atoms on both sites were similar (<5° and <2 kJ mol^{-1} difference) to those that were found for H on each O of isolated sites. Therefore, the initial proton positions on O atoms of second sites were altered to match the relative positions obtained for isolated sites prior to optimization. There are four symmetrically unique O atoms (and thus H binding locations) for each T-site and therefore 16 unique placements in total for both protons on a site-pair. Deprotonation or dehydrogenation can occur on either site, but H atoms were removed only from the first site (the *A* site) because all T-sites are equivalent in CHA. Similar protocols were used to initialize and optimize structures with NH_3 adsorbed to either site or both sites to calculate NH_3 BE values or to calculate the effects of NH_3 adsorption to the second site on the acid strength of the first site.

We examined the effects of unit cell size by combining multiple primitive CHA unit cells into n×1×1 supercells ($n \leq 6$). Structures were optimized until the maximum force on any atom was <0.05 eV Å^{-1} for all calculations performed in CHA supercells. These supercells can be modeled with a constant number of Brønsted acid sites (1) by varying the Si:Al ratio (from 35:1 to 215:1). DPE values for this series increased linearly from 1567 to 1641 kJ mol^{-1} (Figure 3), indicating that either the Al or anion density has a significant effect on DPE values or the artifacts associated with DPE calculations. Supercells were also generated with a constant acid site density and Si:Al ratio (35:1) where only the central site in the supercell was deprotonated to test the effect of anion density, and DPE values for this series also increased linearly from 1567 to 1637 kJ mol^{-1} as the supercell increased from a primitive cell to a 6×1×1 supercell. This indicated that the anion density must play a role in the artifacts associated with DPE calculations. The overlap of the series with a constant number

DOI: 10.1021/acscatal.8b02049
ACS Catal. 2018, 8, 7842−7860

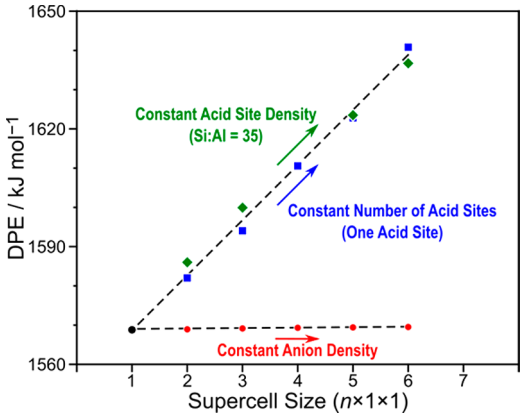

Figure 3. Correlation between supercell size and DPE with a constant acid site density (◆, green), number of acid sites (■, blue), and anion density (●, red). Varying anion density (by holding the number of acid sites or the acid site density constant) leads to artifacts in DPE calculations which correlate linearly with this anion density, while DPE remains constant with constant anion density despite changes in supercell size.

of acids and the constant Si:Al ratio indicate that the Si:Al ratio has no effect on acid strength at these large ratios (≥35:1), suggesting that these sites are "isolated" from one another. Finally, supercells were generated with a constant Si:Al ratio (35) and all sites within the supercell were simultaneously deprotonated to maintain a constant anion density. The resulting DPE values (normalized per proton) were independent of the size of the supercell, demonstrating that the anion density must be kept constant or used as a correction factor for DPE calculations to compare cells of different sizes (Figure 3). This is distinct from previous work[19] which indicated that framework density affected DPE artifacts; however, their application of that correction was successful because framework density correlates strongly with unit cell volume for primitive zeolite unit cells. The supercell calculations done here, however, have identical framework densities, indicating that the true parameter that must be used in these corrections is the density of the anion, which is inversely related to the unit cell volume for DPE calculations involving one deprotonation event. Future work will calculate DPE values in primitive unit cells and variously sized supercells of other zeolite frameworks to determine if the effects of anion density (slope of lines in Figure 3) are similar for other materials, in which case one can accurately compare DPE across different frameworks by correcting the anion density effects.

3. RESULTS AND DISCUSSION

3.1. Predicting the Acid Strength of Isolated Acid Sites in CHA. The CHA framework has four crystallographically unique O atoms (O1−O4, Figure 1c), and each of these O atoms are members of three distinct ring structures. The O1 atom, for example, is a part of the 6MR, the 4MR(1,2), and the 4MR(1,4), where the numbers in parentheses for the 4MRs indicate the O atoms from the *A* site existing in those distinct ring structures. Varying the out-of-plane angle of the proton around the O1 atom (Figure 2) shows minima (stable structures) when the proton is oriented in the plane of one of those rings and the global minimum (most stable structure) orients the proton within the 6MR (Figures 2a and 5a), perhaps because of the relative inflexibility of 4MR structures. The proton weakly H-bonds to other O atoms within the 6MR when it is bound to O1, as indicated by H−O distances of 2.45 and 2.80 Å. Protons bound to O2, O3, and O4 also prefer to orient within the rings associated with those O atoms. The most stable overall proton location is on O1 (oriented in the 6MR), followed in order of decreasing stability by O4, O3, and O2, where it resides in 8MR(2,4), 8MR(2,3), and 8MR(2,3), respectively, with electronic energies relative to the most stable O1 configuration of 2, 4, and 9 kJ mol^{-1} (Figure 4). Reorientations of protons across all O atoms indicate that protons are significantly less stable in the 4MR orientation than in 6MR or 8MR orientations, indicating that significant strain may be induced when orienting a proton inside a 4MR. Protons readily bind to O1, O3, and O4 atoms in CHA, as those energies are within 4 kJ mol^{-1} of one another (within the limits of DFT accuracy), and are less likely to reside on O2 atoms, and this is consistent with previously calculated values using periodic DFT (with the PBE exchange-correlation functional).[19]

The proton is most stable on O1, and therefore the DPE for O1 is the highest of all four O atoms (1572 kJ mol^{-1}; Table 1); it is the least acidic HZ state. The proton located on O2 is the most acidic HZ state and has the lowest DPE (1562 kJ mol^{-1}). Energy calculations on the conjugate base can suffer from charge artifacts inherent in DFT,[52] but there is only one conjugate base structure in the isolated acid site, making these charge artifacts identical for all four HZ states and should not affect identified trends. Previous DFT studies (using PBE) found similarly that H bound to O2 is a stronger acid than the others (O1, O3, O4), which have similar DPE values.[19] In

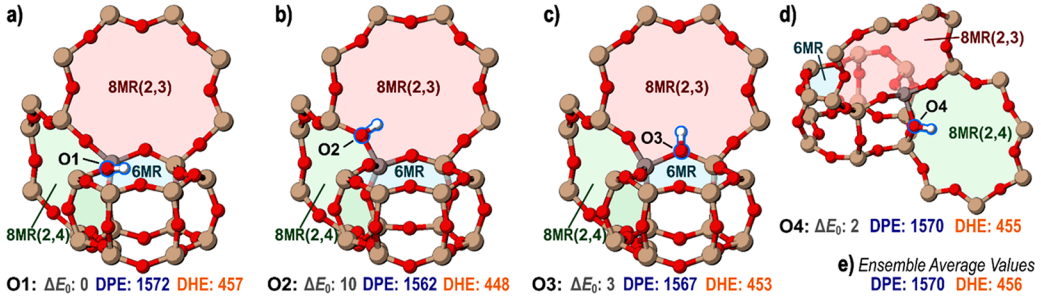

Figure 4. Most stable orientation of the proton on (a) O1, (b) O2, (c) O3, and (d) O4 in the CHA unit cell with only one isolated Brønsted acid site. (e) Ensemble average values of the isolated site for DPE and DHE. The electronic potential energy (ΔE_0) of each state relative to the protonated O1 state is shown, in addition to DPE (eq 3) and DHE (eq 4), in kJ mol^{-1}.

DOI: 10.1021/acscatal.8b02049
ACS Catal. 2018, 8, 7842−7860

Table 1. Electronic Energies (E), Enthalpies (H), and Free Energies (G) for DPE, DHE, and NH_3 BE of Isolated Brønsted Acids in CHA

	DPE			DHE			NH_3 BE		
	E (kJ mol^{-1})	H (kJ mol^{-1})	G (kJ mol^{-1})	E (kJ mol^{-1})	H (kJ mol^{-1})	G (kJ mol^{-1})	E (kJ mol^{-1})	H (kJ mol^{-1})	G (kJ mol^{-1})
O1	1572	1540	1545	457	424	425	−134	−118	−59
O2	1562	1531	1536	448	415	415	−152	−141	−83
O3	1567	1536	1541	453	420	421	−156	−146	−85
O4	1570	1538	1543	455	422	423	−158	−147	−85
arithmetic avg	1568	1536	1541	453	420	421	−150	−138	−78
ensemble avg	1570	1539	1544	456	422	424	−156	−146	−84

experimental environments, protons rapidly move between different oxygens via proton-shuttling species (e.g., H_2O, CH_3OH, NH_3) and form an equilibrated set of proton-form structures.[81] The energy of this equilibrated set of structures can be obtained via ensemble averages (eq 2), which weigh the stability of each HZ state by its relative energy along a Boltzmann distribution. The ensemble average DPE value across the four O atom positions for an isolated Brønsted acid site is 1570 kJ mol^{-1}, close to the DPE of the least acidic HZ states on O1, O3, and O4 (1567−1572 kJ mol^{-1}) because the proton resides on one of these three O atoms 97% of the time according to a Boltzmann distribution of the four relative energies. Therefore, although a proton bound to O2 has the lowest (most acidic) DPE of 1562 kJ mol^{-1}, it becomes catalytically irrelevant because of its relative instability in comparison to a proton bound to O1, O3, or O4.

DHE on an isolated site follows the same trend as DPE and is highest on O1 (457 kJ mol^{-1}) and lowest on O2 (448 kJ mol^{-1}). Figure 5a shows a perfect linear correlation between DPE and DHE for these isolated acid site structures in the CHA unit cell. DPE and DHE are related by

$$\mathrm{DPE} = \mathrm{DHE} + \mathrm{EA} + (E_{H^+} - E_{H\bullet}) \quad (7)$$

The electronic affinity (EA) of the H-depleted framework is the difference in energy of the heterolytically and homolytically cleaved conjugate base:

$$\mathrm{EA} = E_{Z^-} - E_{Z\bullet} \quad (8)$$

The EA is constant for these structures because the location and number of the Al atoms present are not being varied. The ionization energy of hydrogen is the difference in energy between the gas-phase H radical and gas-phase proton, which is also constant. Including these constants yields the linear relation for the isolated acid:

$$\mathrm{DPE} = \mathrm{DHE} + 1115\ (\mathrm{kJ\ mol^{-1}}) \quad (9)$$

Vibrational frequencies for the O−H and Al−O bonds do not significantly depend on the O atom to which the proton is bound. Therefore, zero-point vibrational energies and temperature-corrected vibrational enthalpies and free energies are essentially identical for the four O atom configurations of the isolated acid site, such that DPE and DHE values based on electronic energies are perfectly correlated with values based on enthalpy or free energy values (see Figure S8 in the Supporting Information). Because the relative values of relevant acid strength metrics are not affected by these correction terms, we will report DPE and DHE values in terms of electronic energies throughout the remainder of this work.

Ammonia binding energies (NH_3 BE) measure a mixture of acid strength and confinement effects because the resulting NH_4^+ cation interacts with the local framework. The shift in

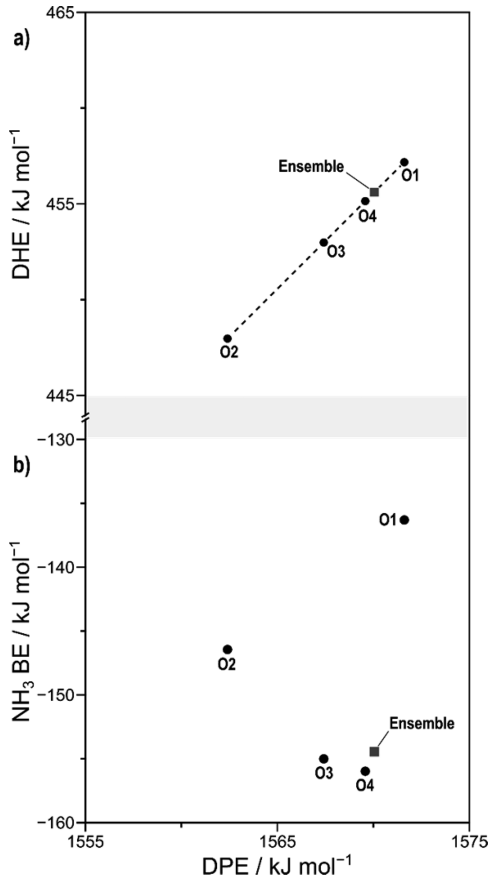

Figure 5. Relationship between (a) DPE and DHE and (b) DPE and NH_3 BE for isolated acid sites. Circles represent values for individual O atoms, and gray squares represent ensemble average values.

confinement effects between a proton and an NH_4^+ cation can alter the preferred orientation of species and confound the relationship between NH_3 BE and acid strength in NH_3 TPD analysis and theoretical assessments.[51,57,62−67] The most stable orientation of the NH_4^+ near an isolated acid site is in the 8MR(2,4) interacting with the O4 atom of the acid site (−158 kJ mol^{-1}) and H-bonding with other framework O atoms (Figures 2c and 6d). The NH_4^+ cation also resides in 8MR structures when it interacts with the O3 (−156 kJ mol^{-1}) and O2 (−152 kJ mol^{-1}) atoms (Figure 6). The O1 atom, however, is not in an 8MR, and when the NH_4^+ cation interacts with that site the binding energy is significantly less exothermic (−134 kJ mol^{-1}), as the resulting NH_4^+ cation resides in the relatively large CHA cage (0.74 nm) rather than in a relatively small 8MR window (0.37 nm). NH_4^+ cations fit well within both 8MR windows of CHA but are too large to fit within the smaller 6MR structures and thus sit above the 6MR

DOI: 10.1021/acscatal.8b02049
ACS Catal. 2018, 8, 7842−7860

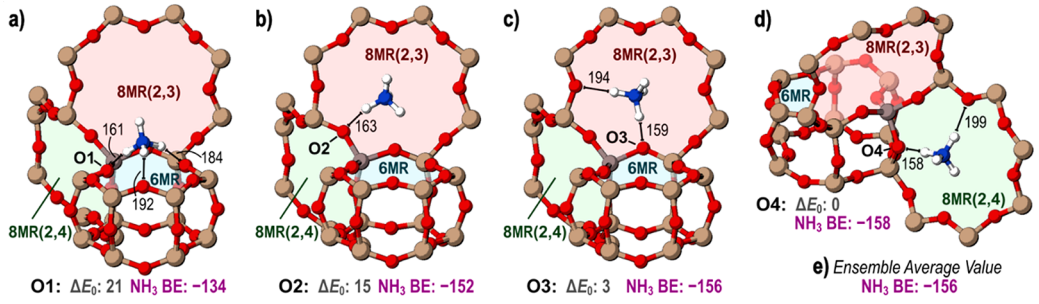

Figure 6. Most stable orientations of adsorbed NH_3 on (a) O1, (b) O2, (c) O3, and (d) O4 of the isolated site. (e) Ensemble average value for NH_3 BE on the isolated site. Interactions between framework O atoms and the NH_4^+ are labeled with their lengths in pm and the NH_3 BE, and electronic potential energy values (ΔE_0) of each state relative to the most stable orientation of bound NH_3 on O4 are shown in kJ mol^{-1}.

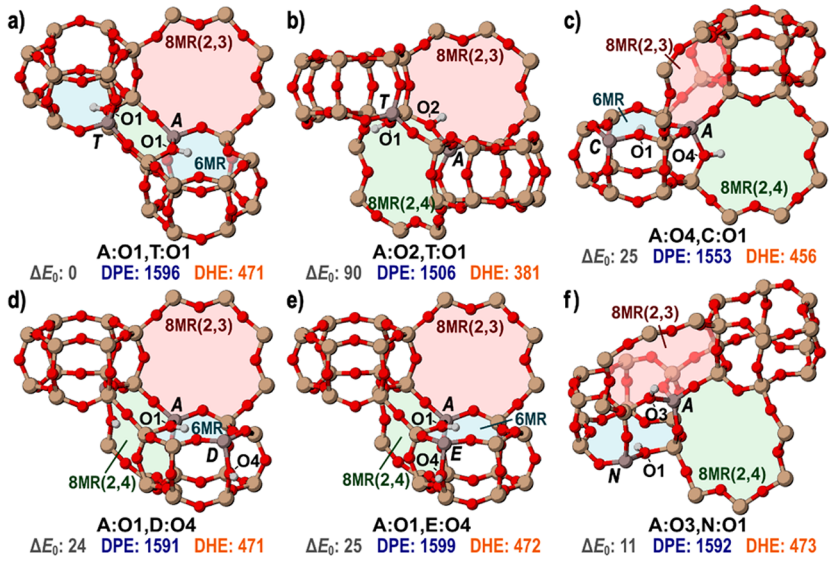

Figure 7. (a) The most stable protonated state for two Al atoms at the *A* and *T* sites (both protons on O1 atoms of each site). (b) The least stable protonated state for the *A* and *T* sites (protons on O2 and O1) in the CHA framework. The most stable configurations of the (c) *A* and *C*, (d) *A* and *D*, (e) *A* and *E*, and (f) *A* and *N* sites are also shown. The energy of each structure is shown below relative to the *A*:O1, *T*:O1 configuration (ΔE_0) with their associated DPE and DHE values in kJ mol^{-1}.

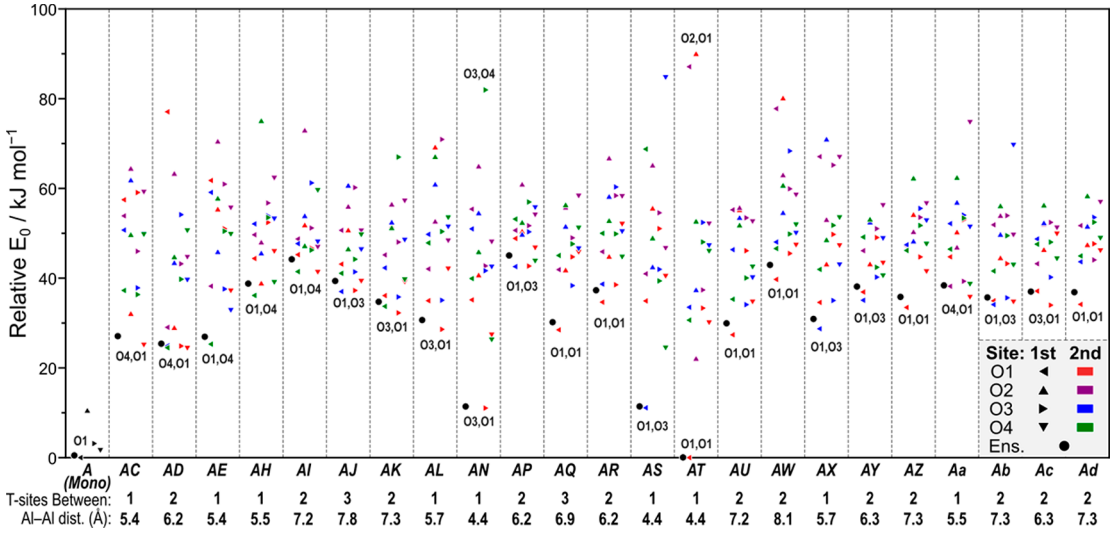

Figure 8. Relative E_0 for protons on the 4 O atoms of isolated sites and the 16 arrangements of protons for all 23 site-pairs shown in kJ mol^{-1}. The distance between Al atoms and the number of Si T-sites linking those sites are shown below. The triangle direction indicates the location of the H on the *A* site: O1 (◀), O2 (▲), O3 (▶), and O4 (▼). The triangle color indicates the location of the H on the second acid site: O1 (red), O2 (purple), O3 (blue), and O4 (green). The ensemble average energy for each site-pair is also shown by a black circle (●). The most stable configuration of protons is labeled for each site-pair, where the location of the proton on the *A* site is listed first.

DOI: 10.1021/acscatal.8b02049
ACS Catal. 2018, 8, 7842−7860

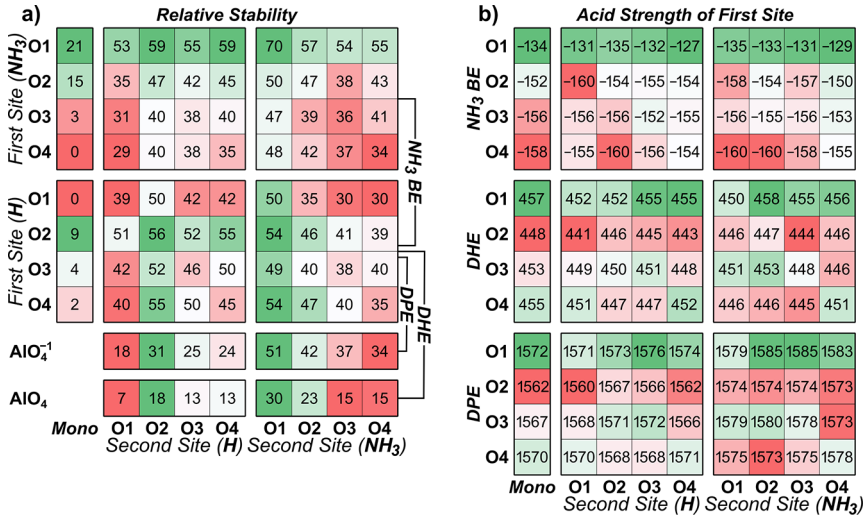

Figure 9. Arithmetic averages for (a) the relative stabilities of the isolated states and of all states averaged across the 23 site-pairs. (b) Values of acid strength measurements for the isolated states and their values for all states averaged across the 23 site-pairs in kJ mol^{-1}.

when interacting with O1. Ammonia is also unlikely to reside inside the di-6MR structure, because the NH_4^+ cation causes significant framework strain, leading to weak binding energies (−100 kJ mol^{-1}). The high stability of the protonated O1 state and poor solvation of the NH_4^+ cation by the CHA cage lead to a less favorable binding of NH_3 to O1 (−134 kJ mol^{-1}) in comparison to the other binding configurations (O2, O3, O4) where NH_3 BE values negatively correlate with DPE or DHE values (Figure 5b), such that weaker acid sites bind NH_3 more strongly, in contrast to expectations. In real systems, however, the position of the proton and NH_4^+ cation are determined by a Boltzmann distribution of the relative stabilities of these species around the Al atom (eq 6) and thus the ensemble average DPE (1570 kJ mol^{-1}), DHE (456 kJ mol^{-1}), and NH_3 BE values (−156 kJ mol^{-1}) are more indicative of catalytic performance than calculations specific to each O atom. These ensemble average predictions of acid strength for isolated Al sites will now be contrasted against similar predictions for sites that have a second Brønsted acid site within one to three "linking" Si T-sites (Figure 1).

3.2. Effects of Acid Site Proximity on Acid Strength. A second Brønsted acid site was created at 23 T-site locations around the *A* site (Figure 1) to determine the effects of proximal sites on acid strength. These additional sites were chosen such that they were separated from the *A* site by one to three T-sites. Protons of each acid site can bind to any one of four O atoms, resulting in 16 total proton configurations for each of the 23 proximal acid site-pairs.

The most stable arrangement of a pair of Brønsted acid sites has Al atoms in the *A* and *T* positions which coexist in the 4MR(1,2) (Figure 1) and with protons on the O1 atoms of each acid site (Figures 7a and 8). In this work, we will denote such an arrangement as *A*:O1, *T*:O1 indicating the location of the two Al atoms (as denoted in Figure 1) and the O atoms to which each proton is bound. The least stable arrangement of a pair of protons is 92 kJ mol^{-1} less stable than *A*:O1, *T*:O1 and also involves Al atoms in the *A* and *T* positions, with protons on the O2 and O1 atoms of the *A* and *T* sites, respectively (*A*:O2, *T*:O1). Protons preferentially bind to O1 atoms of both acids sites in 7 of the 23 arrangements of Al site-pairs (Figure 8); in the remaining arrangements, one proton prefers to bind to an O1 atom while the other binds to either the O3 or O4 atom. The preference of protons to bind to O1 atoms, followed closely by O3 and O4 atoms, is observed for isolated sites (section 3.1), and this trend persists for proximal acid sites. When an arithmetic average of the potential energies relative to the most stable state (*A*:O1, *T*:O1) is taken, the 16 different configurations across 23 arrangements of two Al atoms indicate that protons are most stable on the O1 atoms of proximal sites (average relative *E* of 39 kJ mol^{-1}) and least stable when on O2 atoms (56 kJ mol^{-1}), following trends consistent with those observed for isolated acids (Figure 9a).

Materials with greater amounts of acid site-pairs within the same 6MR (pairs *AC*, *AD*, and *AE*) can be selectively synthesized,[39,40] and such sites can be titrated with Co^{2+} cations such that their kinetic relevance can be independently determined from isolated sites.[39] Preferred proton arrangements on these sites (*AC*, *AD*, *AE*) involve one proton on O1 and oriented into the 6MR; however, two protons cannot favorably coexist within the same 6MR, causing one of the two protons to bind to either an O3 or O4, as shown in Figures 7c−e and 8. These sites (*AC*, *AD*, *AE*) show no remarkable stability or instability in comparison to other Al atom arrangements (Figure 8), indicating that synthesis protocols which increase the likelihood of forming multiple Al atoms within the same CHA cage could form other proximal acid site arrangements, motivating the large number of sites examined in this work and highlighting the need for improved titration and spectroscopic techniques to detect and count such sites.

The acid strength of the first site (position *A*) is estimated by calculating DPE, DHE, and NH_3 BE for all arrangements of protons and bases. The acid strength of the second site is not explicitly calculated because of the equivalent nature of all T-sites in the CHA framework. Deprotonation (or dehydrogenation) of the *A* site leaves that site bare in an anionic (or neutral) form, while the second site has a proton bound to one of its four O atoms. The most stable arrangement of a pair of protons, as discussed, is the *A*:O1, *T*:O1 configuration (Figure 7a), and the *A* site proton has a DPE value of 1596 kJ mol^{-1}, or 26 kJ mol^{-1} higher than that of an isolated site (1570 kJ mol^{-1}), indicating that it is a weaker acid; the least stable configuration of protons is the *A*:O2, *T*:O1 arrangement (Figure 7b), and this results in a strong acid at the *A* site with a DPE value of 1506 kJ mol^{-1}. The stability of the protons and

DOI: 10.1021/acscatal.8b02049
ACS Catal. 2018, 8, 7842−7860

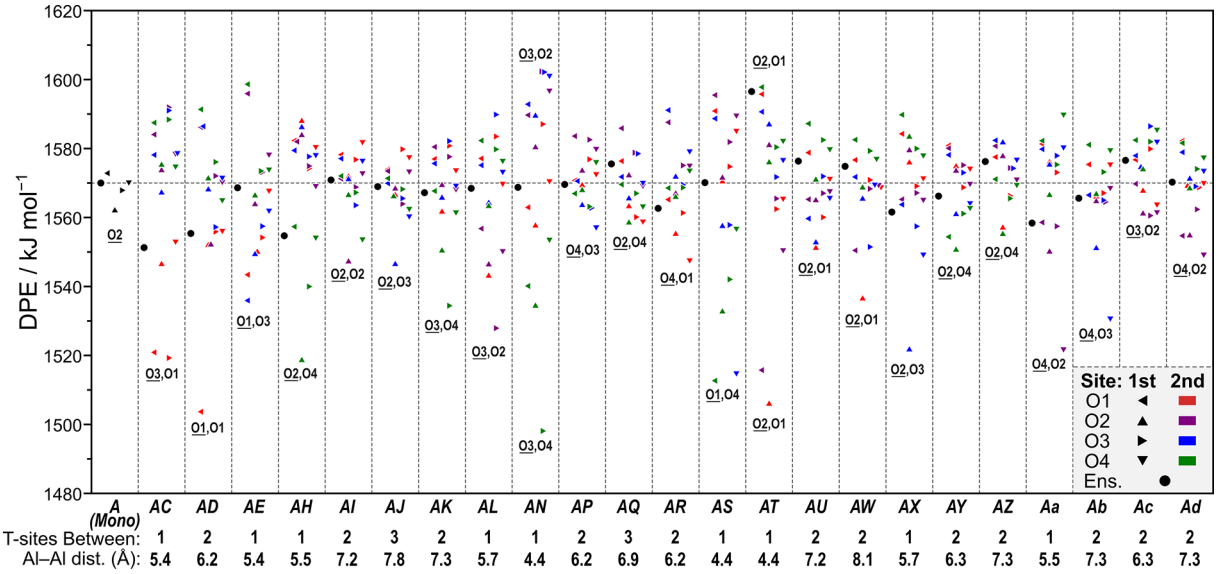

Figure 10. DPE in kJ mol^{-1} for the isolated acid site and all site-pairs where the second site is protonated, with the number of Si linkers between each site and the distance in Å between the Al atoms of each site shown below. The dashed line marks the ensemble average DPE of the isolated site. The location of the most acidic proton combination for each site-pair is marked near its representative point, and the deprotonated O atom on the *A* site is underlined.

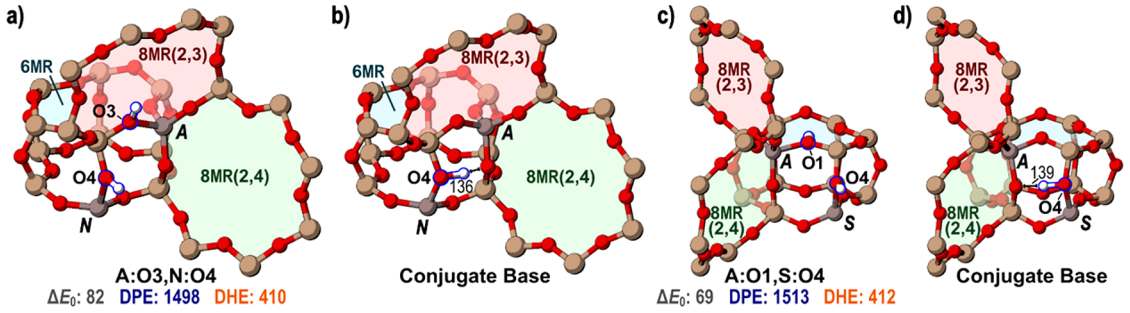

Figure 11. (a) Protons bound to O3 of the *A* site and O4 of the *N* site (*A*:O3, *N*:O4) in this structure giving the lowest DPE value across all structures examined. (b) The most stable conjugate base formed by deprotonation of the *A* site in (a), where the remaining proton interacts strongly with the O4 of the deprotonated site. (c) Protons bound to O1 of the *A* site and O4 of the *S* site also having a low DPE value. (d) The conjugate base exhibiting behavior similar to that of the most stable conjugate base of the *AN* site-pair. The relative stability (ΔE_0), DPE, and DHE values in kJ mol^{-1} are shown beneath the structures which have not been deprotonated, and distances between the remaining H and framework O atoms in the conjugate base structures are shown in pm.

subsequent conjugate base dictate the stability of the proton arrangement.

The proton configurations with the largest and smallest DPE values are both on the *AN* pair, in configurations *A*:O3, *N*:O2 and *A*:O3, *N*:O4 with DPE values of 1602 and 1498 kJ mol^{-1}, respectively (Figure 10). The *A* and *N* sites share a 4MR and are just 4.4 Å apart, and the protons repel one another in the *A*:O3, *N*:O4 configuration, destabilizing the proton on the *A* site (Figure 11a), and decreasing DPE. After deprotonation of the *A* site, the proton remaining on the O4 of the *N* site rotates and forms a strong H-bond (1.36 Å) to the O4 atom of the *A* site, resulting in a very stable conjugate base—the second most stable observed in this work across 92 structures, despite the structural strain induced to accommodate this H-bond configuration (Figure 11b; Figure S1 shows the relative energies of the conjugate base forms). A similar phenomenon occurs on the *AS* site-pair, where the proton on O1 of the *A* site is repelled by the proton on O4 of the *S* site and the subsequent conjugate base rotates to form a strong H bond with O4 of the *A* site, 1.39 Å in length, leading to a strongly acidic arrangement, despite the removal of a proton on O1 of the *A* site and the strain on the framework to accommodate the H-bond (Figure 11c,d). The repulsion of the proton pair and subsequent proton sharing in the conjugate base creates the strong acid at the *A* site, with a DPE value 72 kJ mol^{-1} lower than that of an isolated acid site for the *A*:O3, *N*:O4 arrangement. For most locations of the proximal acid site, the proton sharing between sites that occurs in the formation of the conjugate base at *AN* and *AS* site-pairs cannot occur because larger distances between sites or—in the case of the *AT* site-pair—the energy required to strain the framework for a shared proton exceeds the benefit of the stabilizing effect of the nearby proton, and absent strong interactions between sites, conjugate bases are generally most stable when the remaining proton is on O1 of the second site, mimicking the stabilities of the isolated proton locations. Figure 9a demonstrates that relative energies of protons on the four O atoms of isolated sites are good predictors for the preference of both proton locations in proximal acid sites and of the second proton location in conjugate base structures when these values are

DOI: 10.1021/acscatal.8b02049
ACS Catal. 2018, 8, 7842−7860

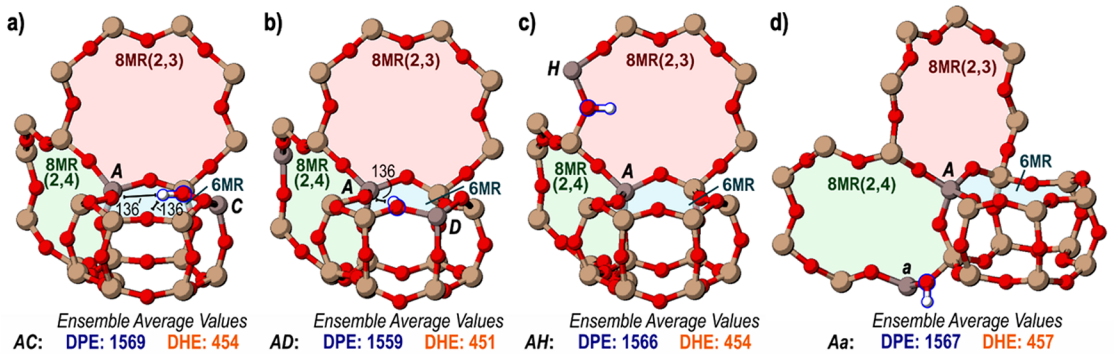

Figure 12. Most stable conjugate bases for site-pairs (a) *AC*, (b) *AD*, (c) *AH*, and (d) *Aa*. Interactions between the proton of the second site and framework O atoms are shown in pm where appropriate. Ensemble average DPE and DHE values for each site-pair are shown below each structure in kJ mol^{-1}.

averaged across the 23 locations of the proximal acid site. A strong acid is one with a weakly bound proton and a stable conjugate base; as such, the lowest average DPE value is predicted when the proton to be removed begins on O2 of the *A* site and the second proton is on O1 of the proximal site, whereas relatively weak *A* site acids are present on the O1 of the *A* site with the second proton on O3 of the proximal site as shown in Figure 9b. These trends indicate how the relative stability of the proton varies across O locations in isolated, proximal, and conjugate base forms, but because of the mobility of these protons, these values are not directly representative of observed acid strength.

The *A*:O2, *T*:O1 and *A*:O3, *N*:O4 arrangements are such strong acids (predicted by DPE), in part, because they are relatively unstable arrangements of protons. The mobility of these protons, however, indicates that they are unlikely to reside in these unstable arrangements, even if they are formed in such arrangements. A proper ensemble average of the 16 proton configurations around Al atoms at both sites and the four configurations of the deprotonated conjugate base structures gives an ensemble DPE value for the *AT* site-pair of 1596 kJ mol^{-1}, 90 kJ mol^{-1} higher than the *A*:O2, *T*:O1 arrangement and 26 kJ mol^{-1} higher (less acidic) than the ensemble DPE of an isolated site. Site-pair *AN*, similarly, has an ensemble DPE value of 1569 kJ mol^{-1}, 71 kJ mol^{-1} higher than the *A*:O3, *N*:O4 configuration and 1 kJ mol^{-1} lower than the ensemble DPE of an isolated site. These examples, applied to Al arranged in the *AT* and *AN* site-pairs, demonstrate the importance of ensemble average DPE values. Unstable arrangements of protons, while having weak O−H bonds and thus low DPE values, rarely exist because of the equilibrated nature of proton transfer among nearby O atoms and this is accounted for by using a Boltzmann distribution for each state (eq 6) within ensemble DPE values. All values reported here are from the RPBE-D3BJ functional, whose trends in ensemble DPE match those of other common functionals used in zeolites (PBE, PBE-D3BJ and BEEF; see the Supporting Information).

The *AC*, *AD*, and *AE* site-pairs within the 6MR of CHA are of particular interest because they can be selectively formed, counted, and thus kinetically tested.[39,40] The *AC* and *AD* site-pairs have ensemble average DPE values lower—1551 and 1555 kJ mol^{-1}, respectively—than that of an isolated site (1570 kJ mol^{-1}). Upon deprotonation of the *A* site, the remaining protons form H-bonds (2.30 and 1.97 Å) across the 6MR to interact with the conjugate base for both the *AC* and *AD* site-pairs (Figure 12a,b), similar to the anion−proton interaction that occurs to stabilize the conjugate base for the *AN* and *AS* site-pairs. The *AE* site-pair has an ensemble DPE value nearly identical (1569 kJ mol^{-1}) to that of the isolated site (1570 kJ mol^{-1}); in its most stable conjugate base configuration, the proton does not reside on O1 but instead on O3 and does not bridge the 6MR to stabilize the deprotonated *A* site. The *AH* and *Aa* site-pairs also have ensemble DPE values (1555 and 1558 kJ mol^{-1}, respectively) lower than that of the isolated site. The *A* and *H* sites are in the same 8MR(2,3), and there is evidence of anion−proton interactions in the conjugate base with a distance of 2.58 Å between the proton and the nearest O atom of the anion (Figure 12c). The conjugate base of the *Aa* site-pair has no close proton−anion interaction, as the proton points away from the *A* site, not toward it (Figure 12d), but the remaining proton is near the *A* site, indicating that a dipole−dipole interaction between the O−H bond of the second site and the Al−O bonds of the anion stabilize the deprotonated site. This sharp reduction in DPE for site-pairs which share rings and are near enough to interact favorably is illustrated by Figure 13, which shows ensemble DPE values for all site-pairs tested. These examples give three distinct methods of stabilizing a conjugate base and therefore decreasing DPE.

Stabilizing the conjugate base is key to decreasing the DPE, and proton−anion distances in the conjugate base structures strongly affect the DPE. Proximal sites for which the remaining proton is near the deprotonated site can form stabilizing proton−anion interactions (H-bonds, dipole−dipole) upon deprotonation and thus have lower DPE values, as shown in Figure 12. Ensemble average DPE values increase with proton−anion distances (as measured by the distance from the proton to the nearest O atom of the anion), and sites with an ensemble average distance in their conjugate bases higher than 4 Å typically have ensemble average DPE values higher than that of the isolated site (Figure 14). Site-pairs *AN* and *AS* have the closest proton−anion interactions (as shown in Figures 11b,d); however, these interactions are present in 4MR structures that have been significantly strained, negating the stabilizing effect of the nearby proton to the conjugate base and resulting in DPE values similar to those of the isolated site. The *AT* site-pair is also present in a 4MR, but its conjugate base does not have a strong anion−proton interaction because the locations of the *A* and *T* sites in the 4MR are not conducive to the proton sharing seen in the *AS* and *AN* site-pairs, which results from the preferred orientation of protons

DOI: 10.1021/acscatal.8b02049
ACS Catal. 2018, 8, 7842−7860

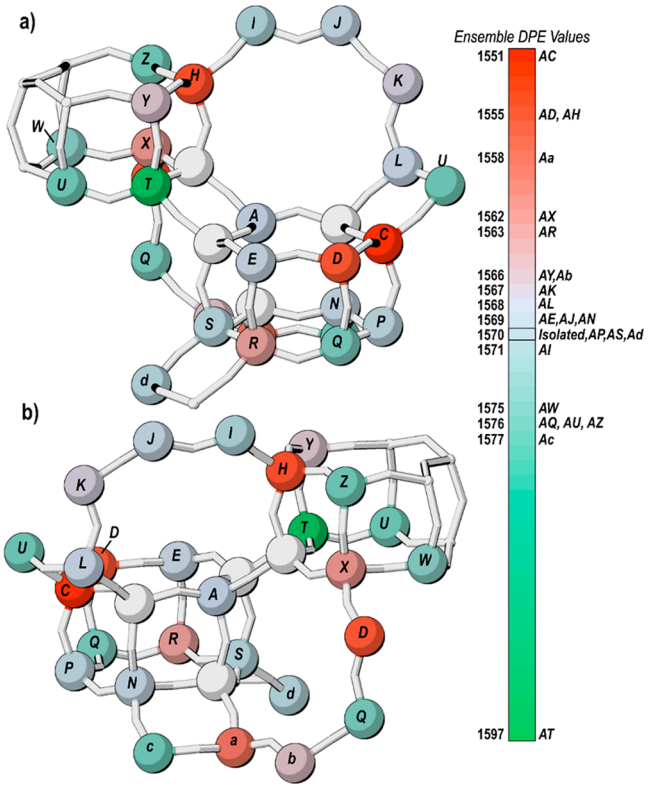

Figure 13. Diagram illustrating the effect of relative framework location on ensemble DPE values for site-pairs showing (a) the 6MR and 8MR(2,3) and (b) the 8MR(2,3) and 8MR(2,4). Site-pairs whose DPE values are higher than that of the isolated site (weaker acids) are shown in green, and those whose DPE values are reduced (stronger acids) are shown in red, with a corresponding color scale and associated ensemble average DPE value on the right.

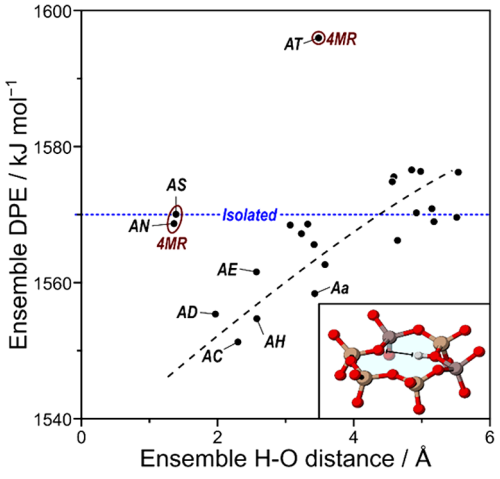

Figure 14. Ensemble average DPE in kJ mol^{-1} as a function of the ensemble average distance in Å between the H of the second site and the nearest O of the deprotonated *A* site. The horizontal dashed line represents the ensemble average value for the DPE of the isolated site, while the sloped dashed line represents a linear fit. The inset at the bottom right shows an example of the shortest H−O distance for the deprotonated *AC* site-pair in the 6MR.

on O1 and O2 of the *T* site, where sharing protons with the *A* site across the 4MR would result in unfavorable strain. Therefore, the DPE of the *AT* site-pair (like sites *AS* and *AN*) is much higher than the trend formed by the remaining 20 site-pairs. After the *AT* site-pair, the *Ac* site-pair has the highest ensemble DPE value (Figure 13). Acid strength can be adjusted by altering the proximity of acid sites, where nearby sites sharing 6MR or 8MR have lower DPE values, and nearby sites sharing 4MR or sites which, upon deprotonation, have a proton and anionic O atom separated by 4 Å or more have higher DPE values.

DHE was also used to probe the acid strength of the *A* site with a second site in the unit cell. The lowest DHE (indicating the weakest O−H bond) is observed for the *A*:O2, *T*:O1 arrangement (381 kJ mol^{-1}), a value 75 kJ mol^{-1} lower than that of the isolated site (456 kJ mol^{-1}). The low DHE of the first site reflects the instability of the H atom on O2; this state is the least stable arrangement of protons and has a low DPE, as previously described. Average DHE values across all proximal site locations for different arrangements of H atoms show similar trends with those from the isolated site; when the proton is on O2, the H−O bond is most easily homolytically cleaved (Figure 9b). Average values across proximal site locations also show strong correlation between DHE and DPE; by both measurements the strongest acids are arranged with a proton on O2 of the *A* site and O1 of the second site and the weakest acids are arranged with a proton on O1 of the *A* site and O3 of the second site.

These values reflect the relative strengths of O−H bonds on various O atoms, but the mobility of H atoms in such systems dictates that ensembled values will reflect their behavior. Ensemble average DHE values for these *AT* and *AS* sites were 471 and 470 kJ mol^{-1}, both higher than the DHE value of an isolated site (456 kJ mol^{-1}), indicating stronger O−H bonds in comparison to that of the isolated site. The DHE values of the *AC*, *AD*, and *AE* site-pairs were 454, 451, and 460 kJ mol^{-1}, which are all similar to the DHE of the isolated site, while their DPE values were lower than that for an isolated site; this indicates that, while a proximal proton can stabilize the conjugate base of the homolytically cleaved H−O bond, the stabilizing benefit conferred by that proton is much stronger when the resulting base is anionic.

A strong trend between ensemble average DPE and ensemble average DHE exists for site-pairs in the CHA unit cell (Figure 15a). The electron affinity (eq 8) for each site-pair differs because sites now interact electronically over shorter distances; therefore, the perfect parity between DPE and DHE on the isolated O atoms disappears. The slope of a linear fit for this relationship is less than 1, indicating that electron affinity decreases when sites share a unit cell and interact. This decrease is an indication of the stabilizing effect that a nearby proton has on a nearby anionic site and offers insight into the increased reactivity for proximal sites where charge separation occurs during reaction.

Ammonia adsorption energies on site *A* were also calculated in the presence of a proximal (protonated) acid site. NH_3 can interact with a proton bound to one of four O atoms at the *A* site, and the second proton can bind to one of four O atoms at the second site, creating 16 unique structures per proximal acid site location. NH_3 deprotonates acid sites, forming an NH_4^+ cation, in all cases. The most stable NH_3 structure is observed when the NH_4^+ cation interacts with the O4 atom of site *A* (in the 8MR(2,4) ring), while the proton of the second site is bound to the O1 atom of site *C* (*A*:O4, *C*:O1), as shown in Figure 16a. The NH_4^+ is stabilized most in the 8MR(2,4), just as was observed for NH_3 bound to the isolated acid site (Figure 6d); in this case, a second proximal proton stabilizes

DOI: 10.1021/acscatal.8b02049
ACS Catal. 2018, 8, 7842−7860

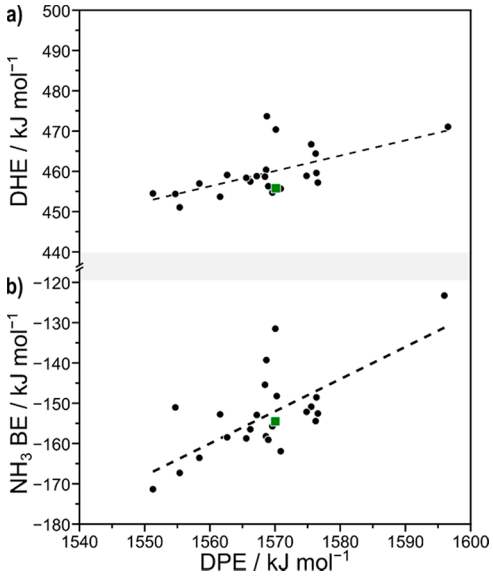

Figure 15. Relationship between (a) DPE and DHE and (b) DPE and NH_3 BE for all site-pairs where the second site is protonated. Energies shown are ensemble averages for each measurement of acid strength in kJ mol^{-1}. Dashed lines represent linear fits, and green squares represent the ensemble average DPE, DHE, and NH_3 BE of the isolated site.

the anionic *A* site across the 6MR upon adsorption of NH_3, as was observed in conjugate base structures after deprotonation (Figure 12). NH_4^+ is similarly stable on the *A*:O4, *D*:O1 site for the same reasons; ammonia adsorption entails heterolytic cleavage of the H−O bond, and the negatively charged Al site is stabilized by proximal protons. NH_3 is least stable when bound to O1 of the *A* site with a nearby proton on the *E* site (Figure 16c). This instability results from unfavorable interactions between the NH_4^+ and the proton. These unfavorable interactions push the proton on O1 of the *E* site into an unstable position above the 6MR, inducing framework strain, much like two protons on the O1 sites of the *AC*, *AD*, and *AE* site-pairs. The stabilization of a bound NH_3 follows trends that are similar to those of NH_3 stability on the isolated site (Figure 9a): it is generally most stable on O4 and least stable on O1. When there is a second proton nearby, the NH_3 is most stable when the proton is on O1 of the second site and least stable when the NH_3 binds to O1 of the *A* site and a proton is on O2 or O4 of the second site.

More exothermic NH_3 BE values are observed when relatively unstable protons create relatively stable NH_4^+ cations upon NH_3 adsorption. The strongest NH_3 adsorption site is the *A*:O3, *N*:O4 site with an NH_3 BE of −208 kJ mol^{-1}; this site also has the highest DPE observed in this work (Figure 16d). While the stabilizing effects of the nearby proton can still affect acid strength measurements, the formation of an extraframework cation which can interact unfavorably with the remaining proton leads to different trends for acid strength of individual combinations of protons for DPE and NH_3 BE (Figure 9b). Because protons and NH_4^+ are mobile, these individual values are not reflective of realistic behavior of these sites, and an ensemble average more accurately reflects the physical properties related to acid strength.

Ensemble average NH_3 BE values for NH_3 bound to the *A* site are most exothermic for site-pairs *AC* and *AD* with values of −171 and −167 kJ mol^{-1}, which are >10 kJ mol^{-1} more exothermic than that of the isolated site (−156 kJ mol^{-1}). Site-pair *AE*, which also involves two sites in the same 6MR, has an ensembled NH_3 BE slightly more exothermic (−158 kJ mol^{-1}) in comparison to isolated sites. The proximal acid in the 6MR stabilizes the deprotonated and anionic *A* site to which NH_3 binds, similar to the stabilization that occurs upon deprotonation to a noninteracting distance (DPE), which also shows that acids are stronger with proximal Al at sites *C* and *D*. Ensemble average NH_3 BE and DPE trend strongly (Figure 15b). This indicates that experimental NH_3 BE measurements, while they can be corrupted by interactions between NH_4^+ cations and the framework, still trend strongly with purely theoretical measurements of acid strength. The strong correlation between NH_3 BE and DPE was not observed in a previous study examining the acid strength of sites across many frameworks;[19] however, changing framework identity or acid site location will significantly alter guest−host interactions between the NH_4^+ cation and the local framework. This study, in contrast, examines the strength of NH_3 adsorption at a single T-site in a single framework and is only altering the presence and location of a proximal acid site, which cause these guest−host interactions to cancel in comparison.

3.3. Sphere of Influence of Acid Sites. To determine the distance at which a second site influences the acid strength of a Brønsted site, DPE and DHE were calculated for 143 Brønsted acid site-pairs in a 4×1×1 CHA supercell. In each orientation, the same centrally located T-site was deprotonated or dehydrogenated. The resulting DPE values were not corrected for their anion densities and are therefore not comparable to

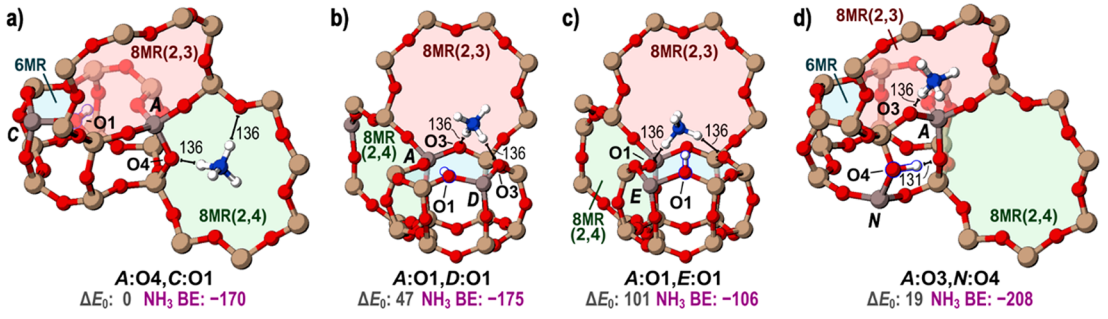

Figure 16. Adsorbed ammonia on (a) O4 of the *A* site with a proton on O1 of the *C* site, (b) O1 of the *A* site with a proton on O1 of the *D* site, (c) O1 of the *A* site with a proton on O1 of the *E* site, and (d) O3 of the *A* site and O4 of the *N* site. Stabilities relative to the *A*:O4, *C*:O1 configuration shown in (a) (ΔE_0) and NH_3 BE for the configuration shown for each site-pair are shown in kJ mol^{-1}. Interactions between H atoms and O atoms of the framework are shown in pm.

DOI: 10.1021/acscatal.8b02049
ACS Catal. 2018, 8, 7842−7860

those calculated for site-pairs in the CHA primitive unit cell but can be compared to one another and thus give insights into the distance over which sites affect each other.

Ensemble DPE values are not well predicted by Al−Al distances, indicating the strong effect of the exact arrangement of Al atoms across different structural motifs (e.g., 6MR, 8MR) as described in preceding sections. With this scatter, Figure 17a also shows a general increase in ensemble DPE values with increasing Al−Al distances as the DPE value increases from ∼1605 kJ mol^{-1} (on average) at distances of 9 Å to ∼1615 kJ mol^{-1} at distances >24 Å along with a concomitant decrease in the scatter, indicating that specific arrangements matter less for sites separated over large distances, as expected. This general increase in DPE values is caused either by shifts in the electron affinity (EA) of the conjugate base or by electronic interactions which exist in charged periodic calculations. EA values are altered by nearby Al atoms; the excess electron is expected to localize at the deprotonated site in this semiconductor material, such that one would expect electron affinities to be governed by local structure (unlike calculations of acid sites on metals which reflect global composition).[27] Alternatively, the long-range effects of Al−Al distance on DPE could be related to the dipole−dipole interactions present for charged periodic calculations that cannot be sufficiently accounted for using these methods. The residual spread in DPE values observed at large distances likely reflects inherent error in DFT methods and does not reflect interactions or differences in T-site locations, as all T-sites are crystallographically identical within the CHA framework.

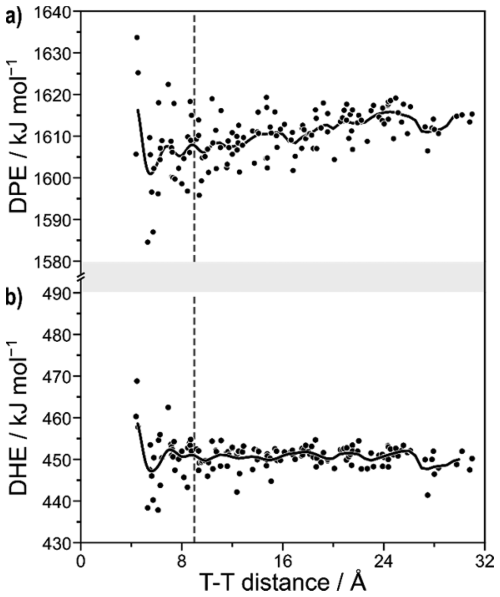

Figure 17. Ensemble average values for (a) DPE and (b) DHE as a function of the distance between Al T-sites in the CHA supercell. The solid black line in each part represents a moving average value for DPE or DHE. Dashed vertical lines represent the 9 Å distance at which site interaction becomes negligible.

Ensemble average DHE values, in contrast to DPE values, are uncorrupted by the large dipole−dipole interactions present in the calculation of charged states in periodic DFT methods. The spread in DHE values, like DPE values, is significant at short distances but rapidly decreases with increasing Al−Al distance (Figure 17b). Unlike DPE, no general increase in DHE values is observed as Al−Al distances increase; ensemble DHE values approach ∼450 kJ mol^{-1} and remain constant, with scatter, across all Al−Al distances >9 Å. Only 13 site-pairs in the supercell have ensemble DHE values which differ by >5 kJ mol^{-1} from this limiting value; 10 of these site-pairs (77%) are separated by <9 Å, despite only 31 of the 143 site-pairs tested in the supercell (22%) being separated by less than 9 Å. The largest variation in DHE values also occurs within this range. Therefore, interactions between sites have the most effect when T-sites are separated by <9 Å.

These data varying the distance between Al sites from 4 to 31 Å provide contradictory sizes for the sphere of influence of an acid site within CHA. DPE values are affected more by proximity than DHE values, with greater scatter and continued shifts in DPE values even at large distances (>20 Å). Such effects, however, cannot be separated from the artifacts inherent in these calculations, and higher methods applied to cluster models of this size are computationally intractable. DHE values, apart from a few outliers, indicate that acid sites do not noticeably interact with one another over distances $\gtrsim$9 Å, roughly corresponding to Al sites separated by three Si T-sites. This cutoff is qualitatively consistent with the effects observed in the primitive CHA unit cell (section 3.2), indicating that Brønsted acids are most affected by the placement of a second site 1−2 T-sites away. As discussed in section 3.5, however, the adsorption of a base (NH_3) to the second site and the subsequent formation of a cation at that site (NH_4^+) that is significantly larger than a proton increases the range over which acid sites interact, leading to significant increases in acid strength for sites within 8MR separated by 3 T-sites (e.g., the *AJ* site-pair, whose Al atoms are separated by 7.8 Å). These data within the 4×1×1 supercell and in the primitive unit cell, taken together, indicate that sites up to ∼9 Å apart, or separated by three T-sites, can influence one another.

3.4. Proximity of Sites with Varying Si:Al Ratios. Bulk Si:Al ratios influence Al−Al distances. Here, we estimate these effects by simulating an Al arrangement assuming a random distribution of Al is generated while obeying Löwenstein's rule[82] such that no two Al are located at adjacent T-sites. Interactions between Brønsted acid sites depend not only on Al−Al distances but also upon the specific arrangement of Al atoms such that no general trend exists between Al−Al distance and shifts in acid strength caused by proximity. However, Figure 17 does indicate that Al−Al distances >9 Å can be considered effectively isolated, while a fraction of Al separated by <9 Å will interact with one another. Figure 18 shows the fraction of Al atoms that have a neighboring Al within 5−16 Å as a function of the Si:Al ratio. For example, 72% of Al atoms have an Al neighbor within 9 Å at a Si:Al ratio of 30, while only 9% have an Al neighbor within 5 Å (across a 4MR in this framework). As Si:Al ratios increase, average Al−Al distances decrease and higher fractions of Al atoms have neighbors at close distances. For example, at a Si:Al ratio of 4 (similar to the case for the chabazite mineral), over 60% of Al atoms have a neighbor within 5 Å. These distance distributions indicate that even high Si:Al ratio materials may have a small fraction of paired sites in the specific arrangements (Figure 13) which alter acid strength. Previous work has more thoroughly investigated the effects of Si:Al ratio on acid strength in FER and similarly found that nearby sites interact with one another at low Si:Al ratios,[61] a finding which is corroborated here. Random distributions of Al sites, however, do not result from

DOI: 10.1021/acscatal.8b02049
ACS Catal. 2018, 8, 7842−7860

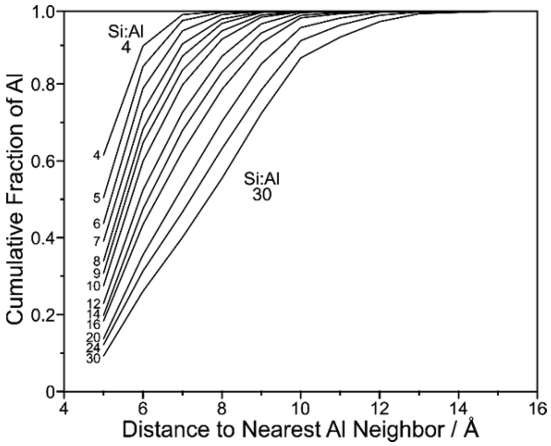

Figure 18. Fraction of sites at a variety of Si:Al ratios with random Al distribution in CHA with nearest Al atoms between 5 and 16 Å away. Curves are labeled on the left with the Si:Al ratio they represent.

target synthesis approaches of more recent investigations,[39,40] but these still give insights into how proximal acid sites in behave in low Si:Al ratio CHA frameworks.

3.5. Altering the State of Proximal Acid Sites. Sections 3.2 and 3.3 considered how a proximal acid site would increase or decrease the strength of the Brønsted acids in CHA. The structures considered in those studies placed a bare proton on the second acid; zeolite-catalyzed reactions, however, rarely occur under conditions that would result in bare protons. Methanol dehydration, for example, occurs on sites covered in a mixture of methanol monomers and dimers, as indicated by kinetic studies showing rates that begin linearly dependent on methanol pressure and approach saturation behavior at higher methanol pressures.[47] This typical Langmuir−Hinshelwood kinetic behavior indicates that the surface composition changes over this range of methanol pressures (0−15.3 kPa CH_3OH) and can be explained by a transition from bare to methanol-covered surfaces or by a transition from surfaces covered in methanol monomers to a surface covered in methanol dimers. The arbiter of this disagreement is in situ FTIR studies that show the complete disappearance of the vibrational signature of bare O−H bonds between 0.2 and 0.5 kPa CH_3OH, indicating that at very low CH_3OH pressures bare protons are not present.[47] The absence of bare protons is also inferred from kinetic data for ethanol dehydration,[22] for arene methylation (and associated reverse-titration experiments),[83] and for alkene oligomerization.[84] This work demonstrates the strong interactions of bare protons with bases, with NH_3 BE values ranging from −106 to −208 kJ mol^{-1} and an ensemble average binding energy on isolated sites of −156 kJ mol^{-1}. These strongly exothermic interactions predict that all surfaces would be covered by NH_3 at low temperatures during any NH_3 TPD study and that such surfaces would likely be covered during relevant catalytic reactions, such as methanol dehydration, which has been previously studied for isolated and paired sites in CHA.[39,47]

Therefore, the effects on the state of the second acid (bare, covered) are critical and were determined here by recalculating DPE, DHE, and NH_3 BE for the same 23 proximal acid site locations with NH_3 adsorbed to the second site. Figure 9b shows that, regarding the arrangements of NH_4^+ cations and protons, similar trends are observed whether the proximal site is a bare proton or deprotonated by NH_3: H is most easily removed from O2 and NH_3 binds most weakly to O1 and most strongly to O4 when NH_3 is bound to the second site. Conclusions can therefore be reached regarding the preferred O binding of protons and NH_4^+ cations similar to those discussed in section 3.2. In this section, we will focus on the effects of the state of the second acid on ensemble average values which reflect the performance of such materials when protons and NH_4^+ cations are mobile.

Adsorbing NH_3 to the proximal site weakens the acid strength of a proton at the *A* site, with ensemble DPE values increasing by an average of 11 kJ mol^{-1}. Bare protons at proximal positions can H-bond to anionic sites in conjugate base structures, and this stabilizing is disrupted in the absence of a bare proton, as the second site has been deprotonated upon contact with NH_3. Considering specifically the *AC*, *AD*, and *AE* site-pairs in which both Al atoms are present in the same 6MR, ensemble DPE values change from 1551, 1555, and 1569 kJ mol^{-1} with a bare proximal proton to 1595, 1588, and 1608 kJ mol^{-1} with a proximal NH_4^+ cation at the nearby *C*, *D*, or *E* site, respectively. These increases of ∼40 kJ mol^{-1} in ensemble DPE suggest that acid site proximity causes acids to weaken in comparison to isolated states (DPE of 1570 kJ mol^{-1}), in direct contrast to the behavior of proximal bare acids, which typically cause these acids to become stronger. Ensemble average DPE values increased upon adsorption of NH_3 to the second site for most site-pairs examined in this study (Figure 19) but decreased by >10 kJ mol^{-1} for the *AJ*,

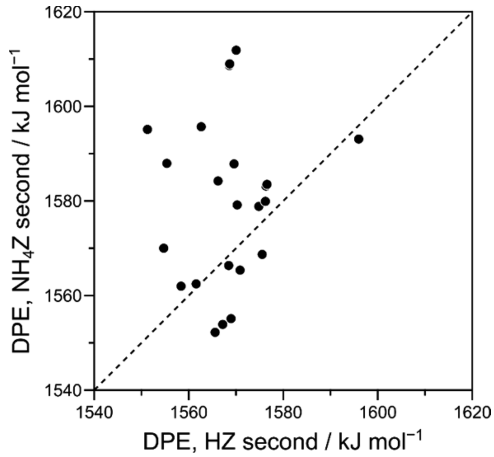

Figure 19. Relationship between DPE values when the second site is protonated (HZ) or when ammonia has adsorbed onto the second site (NH_4Z). The dotted line represents parity between DPE values where the second site is protonated and when NH_3 is bound to the second site.

AK, and *Ab* site-pairs; in each of these cases, acid sites are separated by >7 Å and share an 8MR, indicating the ability of the NH_4^+ cation to stabilize the deprotonated conjugate bases across 8MR structures (Figure 20b−d), similar to the ability of protons to stabilize conjugate base structures across 6MR structures. Sites in the 6MR are stabilized by the NH_4^+ cation similarly to the proton stabilizing the anionic *A* site when it remains protonated; for example, upon deprotonation of the *A* site when NH_3 is adsorbed to the *D* site, the NH_4^+ is no longer located above the 6MR but is pulled down by the anionic *A* site such that it is planar to the 6MR (Figure 20a), but this does not lead to an increase in the stability of the conjugate base. The disruption of the ability of protons to stabilize

DOI: 10.1021/acscatal.8b02049
ACS Catal. 2018, 8, 7842−7860

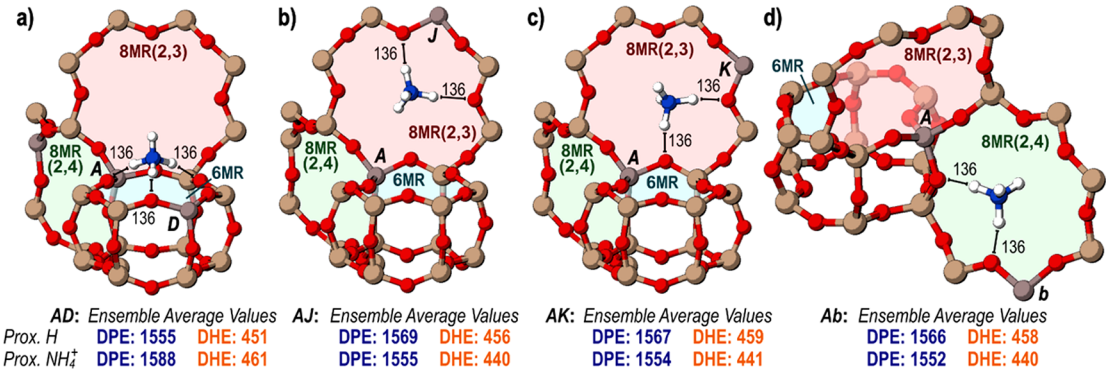

Figure 20. Anions of the (a) *AD*, (b) *AJ*, (c) *AK*, and (d) *Ab* site-pairs with NH_3 adsorbed to the second site. Distances between H of the NH_4^+ and framework O atoms are shown in pm. Ensemble average DPE and DHE values when a H is on the second site and when NH_3 has adsorbed to the second site are shown below each structure in kJ mol^{-1}.

Table 2. Acid Sites Weakened, Unaffected, or Strengthened When a Second Site Is Placed in Varying Positions as a Bare Proton or with NH_3 Adsorbed

		proximal H^+		
		weakened[a] (5)[b]	unaffected (11)	strengthened (6)
proximal NH_4^+	weakened (14)	*AW* (NR, 2)[c]	*AE* (6MR, 1)	*AD* (6MR, 2)
		AZ (NR, 2)	*AN* (4MR, 1)	*AC* (6MR, 1)
		AU (NR, 2)	*AP* (NR, 2)	*AR* (NR, 2)
		Ac (NR, 2)	*AS* (4MR, 1)	
		AT (4MR, 1)	*AY* (NR, 2)	
			Ad (NR, 2)	
	unaffected (4)	*AQ* (8MR, 3)	*AI* (8MR, 2)	*AH* (8MR, 1)
			AL (8MR, 1)	
	strengthened (5)	(none)	*AJ* (8MR, 3)	*AX* (8MR, 1)
			AK (8MR, 2)	*Aa* (8MR, 1)
			Ab (8MR, 2)	

[a]Weakened sites have increased DPE, DHE, and NH_3 BE values (averaged), relative to isolated sites, of >5 kJ mol^{-1}, strengthened sites have values <−5 kJ mol^{-1}, and unaffected sites are within 5 kJ mol^{-1} of isolated sites. [b]The number of site-pairs in each category is shown. [c]Rings shared by the Al in each site-pair are shown in parentheses next to each site-pair along with the number of Si T-sites separating the Al atoms; site-pairs which do not share a ring are marked as "NR".

conjugate base anions across 6MR and over short distances along with the enhanced ability of NH_4^+ cations to stabilize conjugate base anions across 8MR and longer distances results in no strong correlation between ensemble DPE values as the state of the proximal site changes (Figure 19), indicating the need to understand these interactions on a molecular level for each cation (proton or NH_4^+).

DHE can be measured with NH_3 bound to the second site. Much like DPE, the dehydrogenated *A* site is stabilized more strongly by nearby sites which share an 8MR. The *AC*, *AD*, and *AE* site-pairs have DHE values of 470, 466, and 483 kJ mol^{-1}, all higher than the DHE of the isolated site, when the DHE values of *AC* and *AD* with a proton on the second site were lower than the DHE of the isolated site. The DHE of the *AI* (448 kJ mol^{-1}), *AJ* (445 kJ mol^{-1}), *AK* (445 kJ mol^{-1}), *Aa* (440 kJ mol^{-1}), and *Ab* (448 kJ mol^{-1}) site-pairs were all reduced by the presence of NH_3 on the second site, and all of these site-pairs share 8MR. DHE with NH_3 adsorbed to the second site trends strongly with DPE with NH_3 adsorbed to the second site (see the Supporting Information). Again, the perfect parity between the DPE and DHE seen on the isolated site disappears because of the confounding effects of the nearby NH_4^+ cation on the second acid site, which similarly affects the EA of the conjugate bases.

Two adsorbed ammonias are most stable when the first is adsorbed to O4 of the *A* site and the second is adsorbed to O1 of the *D* site. The ammonium cation on the *A* site, when on O4 in the 8MR(2,4), is additionally stabilized by the presence of the *D* site in that ring, which appears due to periodic boundary conditions (Figure 1). The two anionic sites in the 6MR can interact simultaneously with the ammonia adsorbed to O1 of the *D* site, allowing the cation to orient itself more closely to the plane of the ring, rather than the unfavorable interactions of the adsorbed ammonia with the 6MR in the isolated acid (Figure 6a). Because these larger adsorbed species interact differently over longer distances, orientations of ammonia that were unfavorable on the isolated acid and with protonation of the second site can become favorable.

NH_3 binds most favorably binds to O4 of the *A* site when there is NH_3 on O2 of the *W* site (−214 kJ mol^{-1}). Ensemble average NH_3 BE values indicate that NH_3 binds more weakly to the *AC* (−139 kJ mol^{-1}), *AD* (−156 kJ mol^{-1}), and *AE* (−126 kJ mol^{-1}) in comparison to sites separated by longer distances which share 8MR rings with the *A* site, as in the *AI* (−163 kJ mol^{-1}), *AJ* (−165 kJ mol^{-1}), *AK* (−161 kJ mol^{-1}),

DOI: 10.1021/acscatal.8b02049
ACS Catal. 2018, 8, 7842−7860

and *Ab* (−164 kJ mol^{-1}) pairs. Ensemble average values for NH_3 BE also trend linearly with DPE when they are calculated with NH_3 on the second site (Figure S10, see Supporting Information). Arithmetic averages over the location of the first NH_3 indicate that the second NH_3 still generally prefers to bind to O4, with an average adsorption energy of −158 kJ mol^{-1}, and least prefers to bind to O1, with an average adsorption energy of −132 kJ mol^{-1} (Figure 9b).

The average difference between all metrics of acid strength (DPE, DHE, and NH_3 BE) for the isolated site and for a site-pair is used to give a broad view of how a second proximal site can increase, decrease, or have little effect on Brønsted acid strength. Most site-pairs which do not share a ring, or which share a 4MR, are weakened or unaffected by proximity, regardless of the state of the second site (bare or with NH_3 adsorbed; Table 2). Acid sites with a neighbor within the same 6MR are strengthened when the second site is bare but weakened if the second site has NH_3 adsorbed to it. Sites sharing an 8MR can only be strengthened by a bare proton when they are separated by 1 Si T-site, and only site-pairs sharing an 8MR are strengthened by the presence of NH_3 on the second site.

Site-pairs within 6MR structures can be selectively synthesized and titrated and their rates thus independently calculated from isolated sites as shown for CH_3OH dehydration.[39,40] This work demonstrates the abilities of site-pairs in 6MR and 8MR motifs to be stronger acids, depending on their specific arrangement and the adsorbates bound to them. These results can give insights into the enhanced reactivity of increased rates of methanol dehydration on paired sites in CHA.[39] The 4MR, 6MR, and 8MR structural motifs that influence these changes in acid strength with varying Al position also exist in many other zeolite frameworks,[80,85] and Al sites are likely to interact over these similar structural arrangements in many frameworks that contain 6MR and 8MR motifs.

4. CONCLUSION

The proximity of Brønsted acid sites in zeolites alters their strength. This is predicted by DPE, DHE, and NH_3 BE calculations for 23 arrangements of proximal acid sites with varied Al−Al distances in the CHA framework, which has a single crystallographically unique T-site, indicating that all changes in acid strength predictions are related to proximity and not variations in acid site location. Rough correlations were observed among DPE, DHE, and NH_3 BE predictions across all proximal acid sites. Deprotonation of an acid site forms an anionic conjugate base that can be stabilized via H-bonding, dipole−dipole, and electronic interactions by a nearby proton placed one to two linking Si atoms away in specific locations that facilitate such interactions. Acid sites which coexist within 6MR structures of CHA show the greatest enhancement to acid strength, with decreases in ensemble average DPE values of 13−17 kJ mol^{-1}, caused by H-bonding between the conjugate base AlO_4^- and the proximal proton of the second site. These interactions stabilized some conjugate base structures with Al separated by one to two linkers in 8MR arrangements, resulting in slight decreases to DPE values (6−13 kJ mol^{-1}). Brønsted acid sites separated by 1 Si T-site and arranged across a specific 4MR of CHA resulted in very stable protons, and the inability of the residual proton to stabilize the conjugate base results in a calculated DPE value that is ∼30 kJ mol^{-1} higher than that of an isolated site, indicating a significant weakening of the acid; this is the only such arrangement of Al atoms that resulted in an increase in DPE of >10 kJ mol^{-1}. Other sites had weak effects on DPE, with roughly half of all proximal acid sites shifting DPE values by <5 kJ mol^{-1} relative to isolated species.

Brønsted acid sites are rarely unoccupied during catalysis under practical conditions, as protons are typically covered by H-bonding species (e.g., CH_3OH, H_2O), reacted to form surface-bound alkoxides (e.g., CH_3−Z), or deprotonated by a nearby base (e.g., NH_3). Thus, the effect of bare protons on the acid strength of proximal sites may be mitigated by the presence of an adsorbate on that site (e.g., NH_3, CH_3OH) or by the free energy required to desorb that species from the proximal site prior to reaction. A proximal site titrated with NH_3 (forming an NH_4^+ cation) was, for most cases, significantly less capable of stabilizing the conjugate base structure of a nearby acid site, and thus the adsorption of NH_3 to a proximal site increased DPE values of the deprotonated site by 11 kJ mol^{-1}, on average. This shift completely reverses the effects of proximity on acid strength for sites separated by one to two Si in 6MR structures, with DPE values for sites proximal to a second site that is titrated by NH_3 being >20 kJ mol^{-1} higher than those for isolated sites. The NH_4^+ cations present on the second site are not capable of favorably H-bonding to the anionic conjugate base of the first site when these sites are in the same 6MR. Sites separated by two to three Si atoms in the 8MR, however, have conjugate base structures that are stabilized by the NH_4^+ cation (which resides in the plane of the 8MR and H-bonds to both Al sites simultaneously), and these stabilizations result in DPE values that are >10 kJ mol^{-1} lower than isolated sites, indicating an increase in acid strength for these arrangements.

Anionic conjugate base structures of deprotonated acid sites are thus stabilized by proximal protons on Al sites nearby (one to two sites) and across small voids (6MR) which stabilize protons and by proximal NH_4^+ cations on Al sites greater distances away (two to three sites) and across larger voids (8MR) which stabilize NH_4^+ cations. Specific influences of acid site proximity on reaction rates, therefore, will depend on intervening distances and the nature of the voids over which the sites are separated, the state of the second site, and the nature and size of the cation being formed by relevant transition states involved in the reaction.

■ ASSOCIATED CONTENT

Supporting Information

The Supporting Information is available free of charge on the ACS Publications website at DOI: 10.1021/acscatal.8b02049.

Relative energies of anion states, DHE and NH_3 BE values where a proton is on the second site, DPE, DHE, and NH_3 BE with NH_3 bound to the second site, comparison of the DPE values from the RPBE-D3BJ, PBE, PBE-D3BJ, and BEEF functionals, evaluations of *H* and *G* for isolated DPE, DHE, and NH_3 BE, tests for alterations in the convergence criteria and boundary conditions on charged calculations, and trends among DPE, DHE, and NH_3 BE with NH_3 adsorbed to the second site (PDF)

■ AUTHOR INFORMATION

Corresponding Author

*E-mail for D.H.: hibbitts@che.ufl.edu.

DOI: 10.1021/acscatal.8b02049
ACS Catal. 2018, 8, 7842−7860

ORCID

David Hibbitts: 0000-0001-8606-7000

Author Contributions

†S.N. and A.H. contributed equally to this work.

Notes

The authors declare no competing financial interest.

■ ACKNOWLEDGMENTS

The authors gratefully acknowledge helpful discussions with Abdulrahman Almithn (University of Florida), Pavlo Kravchenko (University of Florida), and Mykela DeLuca (University of Florida). The authors gratefully acknowledge funding from ACS Petroleum Research Fund New Doctoral Investigation Award (57079-DNI5). The authors are also grateful for computational resources provided by XSEDE Science Gateways program (CTS160041) and from the University of Florida Research Computing.

■ REFERENCES

(1) Corma, A. Inorganic Solid Acids and Their Use in Acid-Catalyzed Hydrocarbon Reactions. *Chem. Rev.* **1995**, *95*, 559−614.

(2) Corma, A.; Orchillés, A. V. Current Views on the Mechanism of Catalytic Cracking. *Microporous Mesoporous Mater.* **2000**, *35*−*36*, 21−30.

(3) Stöcker, M. Methanol-to-hydrocarbons: Catalytic Materials and Their Behavior. *Microporous Mesoporous Mater.* **1999**, *29*, 3−48.

(4) Chang, C.; Silvestri, A. The Conversion of Methanol and Other O-compounds to Hydrocarbons over Zeolite Catalysts. *J. Catal.* **1977**, *47*, 249−259.

(5) Chang, C. D.; Kuo, J. C. W.; Lang, W. H.; Jacob, S. M.; Wise, J. J.; Silvestri, A. J. Process Studies on the Conversion of Methanol to Gasoline. *Ind. Eng. Chem. Process Des. Dev.* **1978**, *17*, 255−260.

(6) Davis, M. E. Design for Sieving. *Nature* **1996**, *382*, 583−585.

(7) Davis, M. E. Ordered Porous Materials for Emerging Applications. *Nature* **2002**, *417*, 813−821.

(8) Bein, T. Synthesis and Applications of Molecular Sieve Layers and Membranes. *Chem. Mater.* **1996**, *8*, 1636−1653.

(9) Haldoupis, E.; Nair, S.; Sholl, D. S. Pore Size Analysis of > 250,000 Hypothetical Zeolites. *Phys. Chem. Chem. Phys.* **2011**, *13*, 5053−5060.

(10) First, E. L.; Gounaris, C. E.; Wei, J.; Floudas, C. A. Computational Characterization of Zeolite Porous Networks: An Automated Approach. *Phys. Chem. Chem. Phys.* **2011**, *13*, 17339−17358.

(11) Jones, A. J.; Ostrouchov, C.; Haranczyk, M.; Iglesia, E. From Rays to Structures: Representation and Selection of Void Structures in Zeolites Using Stochastic Methods. *Microporous Mesoporous Mater.* **2013**, *181*, 208−216.

(12) Pophale, R.; Cheeseman, P. A.; Deem, M. W. A Database of New Zeolite-like Materials. *Phys. Chem. Chem. Phys.* **2011**, *13*, 12407−12412.

(13) Deem, M. W.; Pophale, R.; Cheeseman, P. A.; Earl, D. J. Computational Discovery of New Zeolite-Like Materials. *J. Phys. Chem. C* **2009**, *113*, 21353−21360.

(14) Jones, A. J.; Zones, S. I.; Iglesia, E. Implications of Transition State Confinement Within Small Voids for Acid Catalysis. *J. Phys. Chem. C* **2014**, *118*, 17787−17800.

(15) Jones, A. J.; Carr, R. T.; Zones, S. I.; Iglesia, E. Acid Strength and Solvation in Catalysis by MFI Zeolites and Effects of the Identity, Concentration and Location of Framework Heteroatoms. *J. Catal.* **2014**, *312*, 58−68.

(16) Gounder, R.; Jones, A. J.; Carr, R. T.; Iglesia, E. Solvation and Acid Strength Effects on Catalysis by Faujasite Zeolites. *J. Catal.* **2012**, *286*, 214−223.

(17) Gounder, R.; Iglesia, E. Catalytic Consequences of Spatial Constraints and Acid Site Location for Monomolecular Alkane Activation on Zeolites. *J. Am. Chem. Soc.* **2009**, *131*, 1958−1971.

(18) Gounder, R.; Iglesia, E. The Roles of Entropy and Enthalpy in Stabilizing Ion-pairs at Transition States in Zeolite Acid Catalysis. *Acc. Chem. Res.* **2012**, *45*, 229−238.

(19) Jones, A. J.; Iglesia, E. The Strength of Brønsted Acid Sites in Microporous Aluminosilicates. *ACS Catal.* **2015**, *5*, 5741−5755.

(20) Carr, R. T.; Neurock, M.; Iglesia, E. Catalytic Consequences of Acid Strength in the Conversion of Methanol to Dimethyl Ether. *J. Catal.* **2011**, *278*, 78−93.

(21) Knaeble, W.; Carr, R. T.; Iglesia, E. Mechanistic Interpretation of the Effects of Acid Strength on Alkane Isomerization Turnover Rates and Selectivity. *J. Catal.* **2014**, *319*, 283−296.

(22) Knaeble, W.; Iglesia, E. Kinetic and Theoretical Insights into the Mechanism of Alkanol Dehydration on Solid Brønsted Acid Catalysts. *J. Phys. Chem. C* **2016**, *120*, 3371−3389.

(23) Macht, J.; Janik, M.; Neurock, M.; Iglesia, E. Catalytic Consequences of Composition in Polyoxometalate Clusters with Keggin Structure. *Angew. Chem.* **2007**, *119*, 8010−8014.

(24) Janik, M. J.; Macht, J.; Iglesia, E.; Neurock, M. Correlating Acid Properties and Catalytic Function: A First-Principles Analysis of Alcohol Dehydration Pathways on Polyoxometalates. *J. Phys. Chem. C* **2009**, *113*, 1872−1885.

(25) Koso, S.; Nakagawa, Y.; Tomishige, K. Mechanism of the Hydrogenolysis of Ethers over Silica-supported Rhodium Catalyst Modified with Rhenium Oxide. *J. Catal.* **2011**, *280*, 221−229.

(26) Chia, M.; Pagán-Torres, Y. J.; Hibbitts, D.; Tan, Q.; Pham, H. N.; Datye, A. K.; Neurock, M.; Davis, R. J.; Dumesic, J. A. Selective Hydrogenolysis of Polyols and Cyclic Ethers over Bifunctional Surface Sites on Rhodium-rhenium Catalysts. *J. Am. Chem. Soc.* **2011**, *133*, 12675−12689.

(27) Hibbitts, D.; Tan, Q.; Neurock, M. Acid Strength and Bifunctional Catalytic Behavior of Alloys Comprised of Noble Metals and Oxophilic Metal Promoters. *J. Catal.* **2014**, *315*, 48−58.

(28) Shinmi, Y.; Koso, S.; Kubota, T.; Nakagawa, Y.; Tomishige, K. Modification of Rh/SiO_2 Catalyst for the Hydrogenolysis of Glycerol in Water. *Appl. Catal., B* **2010**, *94*, 318−326.

(29) Chen, K.; Mori, K.; Watanabe, H.; Nakagawa, Y.; Tomishige, K. C−O Bond Hydrogenolysis of Cyclic Ethers with OH Groups over Rhenium-modified Supported Iridium Catalysts. *J. Catal.* **2012**, *294*, 171−183.

(30) Koso, S.; Watanabe, H.; Okumura, K.; Nakagawa, Y.; Tomishige, K. Comparative Study of Rh−MoOx and Rh−ReOx Supported on SiO_2 for the Hydrogenolysis of Ethers and Polyols. *Appl. Catal., B* **2012**, *111*−*112*, 27−37.

(31) Chatterjee, A.; Iwasaki, T.; Ebina, T.; Miyamoto, A. Density Functional Study for Estimating Brønsted Acid Site Strength in Isomorphously Substituted ZSM-5. *Microporous Mesoporous Mater.* **1998**, *21*, 421−428.

(32) Gounder, R.; Iglesia, E. The Catalytic Diversity of Zeolites: Confinement and Solvation Effects Within Voids of Molecular Dimensions. *Chem. Commun.* **2013**, *49*, 3491−3509.

(33) Bhan, A.; Gounder, R.; Macht, J.; Iglesia, E. Entropy Considerations in Monomolecular Cracking of Alkanes on Acidic Zeolites. *J. Catal.* **2008**, *253*, 221−224.

(34) Wang, S.; Iglesia, E. Catalytic Diversity Conferred by Confinement of Protons Within Porous Aluminosilicates in Prins Condensation Reactions. *J. Catal.* **2017**, *352*, 415−435.

(35) Gounder, R.; Iglesia, E. Effects of Partial Confinement on the Specificity of Monomolecular Alkane Reactions for Acid Sites in Side Pockets of Mordenite. *Angew. Chem., Int. Ed.* **2010**, *49*, 808−811.

(36) Zalazar, M. F.; Paredes, E. N.; Romero Ojeda, G. D.; Cabral, N. D.; Peruchena, N. M. Study of Confinement and Catalysis Effects of the Reaction of Methylation of Benzene by Methanol in H-Beta and H-ZSM-5 Zeolites by Topological Analysis of Electron Density. *J. Phys. Chem. C* **2018**, *122*, 3350−3362.

DOI: 10.1021/acscatal.8b02049
ACS Catal. 2018, 8, 7842−7860

(37) Lesthaeghe, D.; Van Speybroeck, V.; Waroquier, M. Theoretical Evaluation of Zeolite Confinement Effects on the Reactivity of Bulky Intermediates. *Phys. Chem. Chem. Phys.* **2009**, *11*, 5222−5226.
(38) Zicovich-Wilson, C. M.; Corma, A.; Viruela, P. Electronic Confinement of Molecules in Microscopic Pores. A New Concept Which Contributes to the Explanation of the Catalytic Activity of Zeolites. *J. Phys. Chem.* **1994**, *98*, 10863−10870.
(39) Di Iorio, J. R.; Nimlos, C. T.; Gounder, R. Introducing Catalytic Diversity into Single-Site Chabazite Zeolites of Fixed Composition via Synthetic Control of Active Site Proximity. *ACS Catal.* **2017**, *7*, 6663−6674.
(40) Di Iorio, J. R.; Gounder, R. Controlling the Isolation and Pairing of Aluminum in Chabazite Zeolites Using Mixtures of Organic and Inorganic Structure-Directing Agents. *Chem. Mater.* **2016**, *28*, 2236−2247.
(41) Paolucci, C.; Parekh, A. A.; Khurana, I.; Di Iorio, J. R.; Li, H.; Albarracin Caballero, J. D.; Shih, A. J.; Anggara, T.; Delgass, W. N.; Miller, J. T.; Ribeiro, F. H.; Gounder, R.; Schneider, W. F. Catalysis in a Cage: Condition-Dependent Speciation and Dynamics of Exchanged Cu Cations in SSZ-13 Zeolites. *J. Am. Chem. Soc.* **2016**, *138*, 6028−6048.
(42) *Methods of synthesizing chabazite zeolites with controlled aluminum distribution and structures made therefrom*. US Patent US20170107114A1; https://patents.google.com/patent/US20170107114A1/en (accessed Jan 22, 2018).
(43) Dědeček, J.; Sobalík, Z.; Wichterlová, B. Siting and Distribution of Framework Aluminium Atoms in Silicon-Rich Zeolites and Impact on Catalysis. *Catal. Rev.: Sci. Eng.* **2012**, *54*, 135−223.
(44) Knott, B. C.; Nimlos, C. T.; Robichaud, D. J.; Nimlos, M. R.; Kim, S.; Gounder, R. Consideration of the Aluminum Distribution in Zeolites in Theoretical and Experimental Catalysis Research. *ACS Catal.* **2018**, *8*, 770−784.
(45) Yokoi, T.; Mochizuki, H.; Namba, S.; Kondo, J. N.; Tatsumi, T. Control of the Al Distribution in the Framework of ZSM-5 Zeolite and Its Evaluation by Solid-State NMR Technique and Catalytic Properties. *J. Phys. Chem. C* **2015**, *119*, 15303−15315.
(46) Bates, S. A.; Verma, A. A.; Paolucci, C.; Parekh, A. A.; Anggara, T.; Yezerets, A.; Schneider, W. F.; Miller, J. T.; Delgass, W. N.; Ribeiro, F. H. Identification of the Active Cu Site in Standard Selective Catalytic Reduction with Ammonia on Cu-SSZ-13. *J. Catal.* **2014**, *312*, 87−97.
(47) Jones, A. J.; Iglesia, E. Kinetic, Spectroscopic, and Theoretical Assessment of Associative and Dissociative Methanol Dehydration Routes in Zeolites. *Angew. Chem., Int. Ed.* **2014**, *53*, 12177−12181.
(48) Paolucci, C.; Khurana, I.; Parekh, A. A.; Li, S.; Shih, A. J.; Li, H.; Di Iorio, J. R.; Albarracin-Caballero, J. D.; Yezerets, A.; Miller, J. T.; Delgass, W. N.; Ribeiro, F. H.; Schneider, W. F.; Gounder, R. Dynamic Multinuclear Sites Formed by Mobilized Copper Ions in NOx Selective Catalytic Reduction. *Science* **2017**, *357*, 898−903.
(49) Di Iorio, J. R.; Bates, S. A.; Verma, A. A.; Delgass, W. N.; Ribeiro, F. H.; Miller, J. T.; Gounder, R. The Dynamic Nature of Brønsted Acid Sites in Cu−Zeolites During NOx Selective Catalytic Reduction: Quantification by Gas-Phase Ammonia Titration. *Top. Catal.* **2015**, *58*, 424−434.
(50) Paolucci, C.; Verma, A. A.; Bates, S. A.; Kispersky, V. F.; Miller, J. T.; Gounder, R.; Delgass, W. N.; Ribeiro, F. H.; Schneider, W. F. Isolation of the Copper Redox Steps in the Standard Selective Catalytic Reduction on Cu-SSZ-13. *Angew. Chem., Int. Ed.* **2014**, *53*, 11828−11833.
(51) Bates, S. A.; Delgass, W. N.; Ribeiro, F. H.; Miller, J. T.; Gounder, R. Methods for NH_3 Titration of Brønsted Acid Sites in Cu-zeolites That Catalyze the Selective Catalytic Reduction of NOx with NH_3. *J. Catal.* **2014**, *312*, 26−36.
(52) Freysoldt, C.; Neugebauer, J.; Van de Walle, C. G. Fully Ab Initio Finite-size Corrections for Charged-defect Supercell Calculations. *Phys. Rev. Lett.* **2009**, *102*, 016402.
(53) Yuan, S. P.; Wang, J. G.; Li, Y. W.; Jiao, H. Brønsted Acidity of Isomorphously Substituted ZSM-5 by B, Al, Ga, and Fe. Density Functional Investigations. *J. Phys. Chem. A* **2002**, *106*, 8167−8172.
(54) Brand, H. V.; Curtiss, L. A.; Iton, L. E. Computational Studies of Acid Sites in ZSM 5: Dependence on Cluster Size. *J. Phys. Chem.* **1992**, *96*, 7725−7732.
(55) Strodel, P.; Neyman, K. M.; Knözinger, H.; Rösch, N. Acidic Properties of [Al], [Ga] and [Fe] Isomorphously Substituted Zeolites. Density Functional Model Cluster Study of the Complexes with a Probe CO Molecule. *Chem. Phys. Lett.* **1995**, *240*, 547−552.
(56) Svelle, S.; Tuma, C.; Rozanska, X.; Kerber, T.; Sauer, J. Quantum Chemical Modeling of Zeolite-catalyzed Methylation Reactions: Toward Chemical Accuracy for Barriers. *J. Am. Chem. Soc.* **2009**, *131*, 816−825.
(57) Brändle, M.; Sauer, J. Acidity Differences Between Inorganic Solids Induced by Their Framework Structure. A Combined Quantum Mechanics/Molecular Mechanics Ab Initio Study on Zeolites. *J. Am. Chem. Soc.* **1998**, *120*, 1556−1570.
(58) Mallikarjun Sharada, S.; Zimmerman, P. M.; Bell, A. T.; Head-Gordon, M. Insights into the Kinetics of Cracking and Dehydrogenation Reactions of Light Alkanes in H-MFI. *J. Phys. Chem. C* **2013**, *117*, 12600−12611.
(59) Van der Mynsbrugge, J.; Janda, A.; Mallikarjun Sharada, S.; Lin, L.-C.; Van Speybroeck, V.; Head-Gordon, M.; Bell, A. T. Theoretical Analysis of the Influence of Pore Geometry on Monomolecular Cracking and Dehydrogenation Of*n* -Butane in Brønsted Acidic Zeolites. *ACS Catal.* **2017**, *7*, 2685−2697.
(60) Janda, A.; Vlaisavljevich, B.; Lin, L.-C.; Mallikarjun Sharada, S.; Smit, B.; Head-Gordon, M.; Bell, A. T. Adsorption Thermodynamics and Intrinsic Activation Parameters for Monomolecular Cracking Of *n*-Alkanes on Brønsted Acid Sites in Zeolites. *J. Phys. Chem. C* **2015**, *119*, 10427−10438.
(61) Grajciar, L.; Areán, C. O.; Pulido, A.; Nachtigall, P. Periodic DFT Investigation of the Effect of Aluminium Content on the Properties of the Acid Zeolite H-FER. *Phys. Chem. Chem. Phys.* **2010**, *12*, 1497−1506.
(62) Suzuki, K.; Sastre, G.; Katada, N.; Niwa, M. Ammonia IRMS-TPD Measurements and DFT Calculation on Acidic Hydroxyl Groups in CHA-type Zeolites. *Phys. Chem. Chem. Phys.* **2007**, *9*, 5980−5987.
(63) Lercher, J. A.; Gründling, C.; Eder-Mirth, G. Infrared Studies of the Surface Acidity of Oxides and Zeolites Using Adsorbed Probe Molecules. *Catal. Today* **1996**, *27*, 353−376.
(64) Katada, N.; Suzuki, K.; Noda, T.; Sastre, G.; Niwa, M. Correlation Between Brønsted Acid Strength and Local Structure in Zeolites. *J. Phys. Chem. C* **2009**, *113*, 19208−19217.
(65) Parrillo, D. J.; Gorte, R. J. Characterization of Acidity in H-ZSM-5, H-ZSM-12, H-Mordenite, and H-Y Using Microcalorimetry. *J. Phys. Chem.* **1993**, *97*, 8786−8792.
(66) Gorte, R. J. What Do We Know About the Acidity of Solid Acids? *Catal. Lett.* **1999**, *62*, 1−13.
(67) Gorte, R. Design Parameters for Temperature Programmed Desorption from Porous Catalysts. *J. Catal.* **1982**, *75*, 164−174.
(68) Demmin, R.; Gorte, R. J. Design Parameters for Temperature-programmed Desorption from a Packed Bed. *J. Catal.* **1984**, *90*, 32−39.
(69) Kresse, G.; Furthmüller, J. Efficiency of Ab-initio Total Energy Calculations for Metals and Semiconductors Using a Plane-wave Basis Set. *Comput. Mater. Sci.* **1996**, *6*, 15−50.
(70) Kresse, G.; Furthmüller, J. Efficient Iterative Schemes for Ab Initio Total-energy Calculations Using a Plane-wave Basis Set. *Phys. Rev. B: Condens. Matter Mater. Phys.* **1996**, *54*, 11169−11186.
(71) Kresse, G.; Hafner, J. Ab Initio Molecular-dynamics Simulation of the Liquid-metal-amorphous-semiconductor Transition in Germanium. *Phys. Rev. B: Condens. Matter Mater. Phys.* **1994**, *49*, 14251−14269.
(72) Kresse, G.; Hafner, J. Ab Initio Molecular Dynamics for Liquid Metals. *Phys. Rev. B: Condens. Matter Mater. Phys.* **1993**, *47*, 558−561.
(73) Blöchl, P. E. Projector Augmented-wave Method. *Phys. Rev. B: Condens. Matter Mater. Phys.* **1994**, *50*, 17953−17979.

DOI: 10.1021/acscatal.8b02049
ACS Catal. 2018, 8, 7842−7860

(74) Kresse, G.; Joubert, D. From Ultrasoft Pseudopotentials to the Projector Augmented-wave Method. *Phys. Rev. B: Condens. Matter Mater. Phys.* **1999**, *59*, 1758−1775.
(75) Hammer, B.; Hansen, L. B.; Nørskov, J. K. Improved Adsorption Energetics Within Density-functional Theory Using Revised Perdew-Burke-Ernzerhof Functionals. *Phys. Rev. B: Condens. Matter Mater. Phys.* **1999**, *59*, 7413−7421.
(76) Grimme, S.; Ehrlich, S.; Goerigk, L. Effect of the Damping Function in Dispersion Corrected Density Functional Theory. *J. Comput. Chem.* **2011**, *32*, 1456−1465.
(77) Wellendorff, J.; Lundgaard, K. T.; Møgelhøj, A.; Petzold, V.; Landis, D. D.; Nørskov, J. K.; Bligaard, T.; Jacobsen, K. W. Density Functionals for Surface Science: Exchange-correlation Model Development with Bayesian Error Estimation. *Phys. Rev. B: Condens. Matter Mater. Phys.* **2012**, *85*, 235149.
(78) Brogaard, R. Y.; Moses, P. G.; Nørskov, J. K. Modeling van Der Waals Interactions in Zeolites with Periodic DFT: Physisorption of *n*-Alkanes in ZSM-22. *Catal. Lett.* **2012**, *142*, 1057−1060.
(79) Perdew, J. P.; Burke, K.; Ernzerhof, M. Generalized Gradient Approximation Made Simple. *Phys. Rev. Lett.* **1996**, *77*, 3865−3868.
(80) Baerlocher, C.; McCusker, L. B. Database of Zeolite Structures; http://www.iza-structure.org/.
(81) Ryder, J. A.; Chakraborty, A. K.; Bell, A. T. Density Functional Theory Study of Proton Mobility in Zeolites: Proton Migration and Hydrogen Exchange in ZSM-5. *J. Phys. Chem. B* **2000**, *104*, 6998−7011.
(82) Löwenstein, W. The Distribution of Aluminum in the Tetrahedra of Silicates and Aluminates. *Am. Mineral.* **1954**, *39*, 92−96.
(83) Hill, I.; Malek, A.; Bhan, A. Kinetics and Mechanism of Benzene, Toluene, and Xylene Methylation over H-MFI. *ACS Catal.* **2013**, *3*, 1992−2001.
(84) Sarazen, M. L.; Iglesia, E. Stability of Bound Species During Alkene Reactions on Solid Acids. *Proc. Natl. Acad. Sci. U. S. A.* **2017**, *114*, E3900−E3908.
(85) Baerlocher, C.; McCusker, L. B.; Olson, D. H. *Atlas of Zeolite Framework Types*; 6th ed.; Elsevier, 2007.

DOI: 10.1021/acscatal.8b02049
ACS Catal. 2018, 8, 7842−7860